

Chemical characterization of wintertime marine aerosols over the Arabian Sea: impact of marine sources and long-range transport

Poonam Bikkina^{1,*}, V.V.S.S. Sarma¹, Kimitaka Kawamura², Srinivas Bikkina², Bhagawati Kunwar², Sherin C.K.³

¹CSIR-National Institute of Oceanography, Regional Centre,
Visakhapatnam 530017, Andhra Pradesh, India

²Chubu University, Kasugai-shi, Aichi, 487-8501, Japan

³Center for Marine Living Resources and Ecology, Kochi 682508, Kerala, India

*Corresponding author: Dr. Poonam Bikkina (ptyagi@nio.res.in)

Abstract

We examined here the compositional characteristics of total suspended particulate (TSP) samples collected along the east coast of the Arabian Sea during a winter cruise (SS379: 6-26 December 2017) to understand the extent of influence of air pollutants from terrestrial sources. The samples (N = 17) were analyzed for water-soluble inorganic species (WSIS), elemental carbon (EC), organic carbon (OC) and water-soluble carbon (WSOC). Backward air mass trajectories and satellite-based fire counts revealed an influence of long-range transport of biomass burning emissions in the Indo-Gangetic Plain and southern India. Anthropogenic (82-97%) SO_4^{2-} is the most abundant WSIS followed by Na^+ and/or NH_4^+ . Ambient EC loadings ($0.5 - 2.4 \mu\text{g m}^{-3}$) and OC/EC ratios (2.5-10.5) are higher than usually expected for fossil-fuel combustion sources. Low mass ratios of $\text{NO}_3^-/\text{non-sea-salt SO}_4^{2-}$ (0.08-0.49), as well as high ratios of $\text{nss-K}^+/\text{EC}$ (0.14-1.18) and WSOC/OC (0.30-0.74), highlight the significance of coal combustion and biomass burning emissions in the regional influx of air pollutants to the Arabian Sea. The multiple linear regression analysis indicated strong correlations among sea salt components (Na^+ , Cl^- and Mg^{2+}), carbonaceous components (OC, EC and WSOC), and anthropogenic WSIS (NH_4^+ and SO_4^{2-}). Furthermore, we used minimum R-squared technique based primary OC/EC ratio in the EC-tracer method to estimate the contribution of secondary organic carbon (SOC) to OC (7-61%) and TSP mass (0.7-11%). Overall, the composition of TSP is characterized by $21 \pm 10\%$ of particulate organic matter, $2.3 \pm 1.1\%$ of EC, $21 \pm 9\%$ of anthropogenic WSIS and $43 \pm 15\%$ of unidentified fraction including dust. This study has implications for understanding the evolving nature of secondary inorganic and organic aerosols in the continental outflows.

Keywords: Chemical composition, Arabian Sea, coastal aerosols, Indo Gangetic Plain, southern India.

1. Introduction

Atmospheric carbonaceous species and other particulate matter significantly influence the regional climate directly by scattering or absorbing sunlight and indirectly by modifying hygroscopic and cloud condensation nuclei activity of aerosols and thus, microphysical properties of clouds (Menon et al., 2002; Bond and Bergstrom, 2006; Ramanathan and Carmichael, 2008; Andreae and Ramanathan, 2013; Hu et al., 2017). In recent years, growing emission of carbonaceous aerosols from the Asian region is a major concern in the developing nations because of their associated health and climate effects (Venkataraman et al., 2005; Satheesh et al., 2008; Gustafsson et al., 2009; Krishna Moorthy et al., 2013; Marlier et al., 2013; Cong et al., 2015). Some of the climate-effects carbonaceous aerosols include the frequent occurrence of storms, increase in droughts, delay in the onset of monsoon, affecting the precipitation patterns, extent of glaciers and hydrological cycle (Seinfeld et al., 2004; Lau et al., 2006; Burney and Ramanathan, 2014; Fadnavis et al., 2019). However, these projected effects are more uncertain mainly because of the limited information on emission characteristics and evolution of carbonaceous aerosols and their mixing with other chemical species during long-range transport (Srivastava et al., 2012; Cong et al., 2015; Gustafsson and Ramanathan, 2016; Hu et al., 2017). More importantly, there is a dearth of knowledge on the relative significance of organic aerosols (OA) emitted directly from the sources versus those formed by the secondary formation processes in terms of their role in influencing the regional radiative forcing of soot particles in the atmosphere (Ramana et al., 2010; Gogoi et al., 2017; Thamban et al., 2017).

Coastal seas and remote oceans are vulnerable to the continental pollution during the northeast monsoon (Lelieveld et al., 2001; Ramanathan et al., 2001; Zhang et al., 2007; Balasubramanian et al., 2013). In particular, the widespread haze pollution in winter season caused by the anthropogenic source-emissions in the Indo-Gangetic Plain (IGP) and southern India have been shown to influence the chemical composition of aerosols over the downwind oceanic regions during the winter period (Kumar et al., 2008a; Kumar et al., 2008b; Sudheer and Sarin, 2008; Sarin et al., 2010; Kumar et al., 2012; Bikkina and Sarin, 2013; Bikkina et al., 2014; Alam et al., 2018; Bikkina et al., 2019b; Aswini et al., 2020). This is because of the more stagnant weather conditions (*i.e.*, less turbulence), shallow atmospheric boundary layer altogether accumulates air pollutants, which are eventually long-range transported by the prevailing northeast monsoonal winds (Nair et al., 2007; Bikkina et al., 2019a)

Preliminary investigations have suggested a stronger influence of anthropogenic source-emission on the marine atmosphere of the Bay of Bengal (an eastern limb of the northern Indian Ocean) as compared to its western counterpart, the Arabian Sea (Kumar et al., 2008b; Bikkina and Sarin, 2012). All these inferences so far have relied upon the comparison of the chemical

composition of aerosols collected over these basins during different seasons. Such data give limited information as each campaign from the ocean is a snapshot and represents compositional characteristics of marine aerosols under different pollution regimes. Therefore, an effort has been made to better characterize the chemical composition of wintertime aerosols over the Arabian Sea. Here we measured the mass concentrations of carbonaceous species and water-soluble inorganic ions in the total suspended particulate matter (TSP) aerosols from this marine basin during a winter cruise (6-24 December 2018). The objectives of this study are (i) to assess the mass concentrations of carbonaceous and water-soluble inorganic species (WSIS) in marine aerosols over the coastal Arabian Sea and (ii) to compare the chemical composition in terms of their diagnostic mass ratios between the Arabian Sea and the Bay of Bengal under similar conditions (*i.e.*, winter data). Here, we discuss major differences between the two oceans in terms of the sources and transport patterns of airborne particulate matter during the continental outflow.

2. Materials and Methods

2.1. Cruise track and meteorology

The Arabian Sea is a semi-enclosed marine basin characterized by high surface salinity and less riverine input, being in contrast to its eastern counterpart, the Bay of Bengal. Besides, the Arabian Sea receives air pollutants during the winter season from northern India as evident by the high aerosol optical depth (AOD) (*i.e.*, retrieved from the moderate resolution imaging spectroradiometer (MODIS) satellite) because of the prevailing northeasterly trade winds (Figure 1a; wind fields were obtained from this web URL <https://psl.noaa.gov/data/gridded/data.ncep.reanalysis.pressure.html>). The wind speed and direction data, obtained from the ship's automatic weather station (AWS), also clearly revealed that surface winds are mostly from the northeast direction (Figure 1b). No precipitation events were observed during the cruise in the Arabian Sea. The daily mean temperature and relative humidity during the SS379 cruise varied from 22.1 °C to 29.7 °C (av. 27.3 °C) and 42.5% to 72.1% (av. 57.5%), respectively. We collected the TSP samples onboard FORV Sagar Sampada (SS379), a research vessel dedicated for fostering scientific research in the marginal seas by the Ministry of Earth Sciences (MoES), India. The cruise was conducted in the offshore waters of the Arabian Sea, started from Kochi on 6 December 2018 and ended at Okha port in Gujarat on 25 December 2018.

2.2. Aerosol collection and analysis

Seventeen aerosol samples were collected on 8"× 10" precombusted (at 450°C for 6 h) PALLFLEX[®]™ Tissuquartz filters using a high volume air sampler (TSP, Envirotech Pvt. Ltd.),

which was setup on the front deck of ship's navigation room at a height of 10 m above the sea level. The sampler was operated only when the ship is cruising at a speed of 10 knots per hour and winds are coming from the bow side to avoid any contamination from the ship exhaust. The sampler was calibrated before and after the cruise to ascertain any variations in the flowrate and was found to be within 5% of standard nominal value ($1.13 \text{ m}^3 \text{ min}^{-1}$). The sampled air volumes varied between 233 and 2324 m^3 (av. 1642 m^3). After collection, TSP samples were wrapped in precombusted aluminium foils, sealed in airtight Ziploc bags and stored at $-20 \text{ }^\circ\text{C}$ until further chemical analysis. Along with samples, five field blanks were collected without running the pump to ascertain any contamination associated with handling and storage.

A $\sim 2.0 \text{ cm}^2$ filter punch of aerosol sample was extracted with ultrapure deionized water (Milli-Q; specific resistivity $> 18.2 \text{ M}\Omega\text{-cm}$) using ultrasonic agitation ($10 \text{ ml} \times 10 \text{ min}$; 3 cycles). The extracts were subsequently filtered through a $0.22 \text{ }\mu\text{m}$ syringe filter (PVDF; Millex-Millipore). This water extract was analyzed for major anions (Cl^- , NO_3^- and SO_4^{2-}) and cations (Na^+ , NH_4^+ , K^+ , Ca^{2+} and Mg^{2+}) using isocratic elution on Metrohm ion chromatograph (IC761) connected in line with both anion and cation columns (Shodex-resin). While anions were eluted with a mixture of solutions containing $1.8 \text{ mM Na}_2\text{CO}_3$ and 1.7 mM NaHCO_3 , whereas cations were eluted with a mixture of solutions containing 5 mM tartaric acid, 1 mM dipicolinic acid and 24 mM boric acid. Calibrations were performed daily with the gravimetrically prepared standards from high purity target chemical substances. Field blanks were also extracted and analyzed for the target analytes on the ion chromatograph in a similar fashion to that of aerosol samples. Blank signals were 10 times lower than the minimum concentration found in the samples. Based on the repeat analysis of standards, the overall analytical reproducibility in the mass concentrations of anions and cations is ascertained to be within 6% for our study. The method detection limits (MDL) for the WSIS analyzed on the ion chromatograph were considered here as three times the standard deviation of procedural field filter blanks normalized to the average volume of air filtered for the TSP samples collected over the Arabian Sea. The MDL are $0.070 \text{ }\mu\text{g m}^{-3}$ for Na^+ , $0.061 \text{ }\mu\text{g m}^{-3}$ for NH_4^+ , $0.113 \text{ }\mu\text{g m}^{-3}$ for K^+ , $0.01 \text{ }\mu\text{g m}^{-3}$ for Ca^{2+} , $0.01 \text{ }\mu\text{g m}^{-3}$ for Mg^{2+} , $0.023 \text{ }\mu\text{g m}^{-3}$ for MSA^- , $0.15 \text{ }\mu\text{g m}^{-3}$ for Cl^- , $0.10 \text{ }\mu\text{g m}^{-3}$ for NO_3^- , and $0.062 \text{ }\mu\text{g m}^{-3}$ for SO_4^{2-} .

Another circular filter punch of 16 mm diameter was analyzed for elemental carbon (EC) and organic carbon (OC) on a semicontinuous carbon analyzer (Sunset Laboratory, SF, CA) using the national institute for occupational health and safety (NIOSH 5040) protocol. The analytical accuracy of the instrument was ascertained by analyzing the gravimetrically prepared sucrose and potassium hydrogen phthalate standards for their total carbon content. No detectable signal was observed for

EC in the procedural filter blanks and, hence, no correction was applied for estimating its mass concentration in TSP samples. The average OC concentration in the procedural filter blanks (N =3) was less than $1.91 \pm 0.4 \mu\text{g cm}^{-2}$, which is four times lower than the minimum signal observed for the samples. Based on the repeat analysis of samples, the overall external reproducibility was 5% for OC and 10% for EC. For the mass concentration of WSOC, $\sim 10 \text{ cm}^2$ area of filter sample was extracted with Milli-Q water by ultrasonic treatment and filtered through $0.22 \mu\text{m}$ syringe filter (Millex-GV). This extract was analyzed for nonpurgeable organic carbon (NPOC) on the total organic carbon (TOC, Shimadzu model) analyzer, which was calibrated using gravimetrically prepared potassium hydrogen phthalate standard solutions. We found that replicate analyses of filter samples yielded an overall external precision of $\sim 10\%$ for WSOC. Additionally, we also analyzed another external standard ($\sim 1.4 \text{ ppm-C}$ of L-Aspartic acid) to ascertain the accuracy of the calibration and the results from the TOC analyzer showed agreement within 4.8%.

2.3. Backward air mass trajectories and fire count data

To ascertain the probable source regions contributing to TSP composition, seven-day isentropic backward air mass trajectories were computed using the hybrid single-particle lagrangian integrated trajectory model (HYSPLIT, version-4) (Draxler and Rolph, 2009; Stein et al., 2015). For this, we used archived meteorological datasets from the National Centers For Environmental Prediction (NCEP)-National Centre For Atmospheric Research (NCAR) (*i.e.*, available from the web portal, https://ready.arl.noaa.gov/HYSPLIT_traj.php) as an input file to the HYSPLIT model. Furthermore, the firecount data was obtained from the moderate resolution imaging spectroradiometer (MODIS) satellite retrievals using Giovanni online webportal (<https://giovanni.gsfc.nasa.gov/giovanni/>), maintained by the National Aeronautics and Space Administration (NASA) to assess the impact of biomass burning emission on the composition of TSP over the Arabian Sea. The firecount data was combined with backward air mass trajectories when discussing the temporal variability of chemical constituents in TSP collected along the cruise track (Figure 1a).

3. Results and discussion

3.1. Temporal variability of ionic species and carbonaceous components

Concentrations of TSP over the Arabian Sea exhibited pronounced temporal variability during the winter cruise ($28\text{-}232 \mu\text{g m}^{-3}$). Accordingly, such variability is also reflected in the mass loadings of WSIS and carbonaceous components in TSP (Table 1). To assess the impact of anthropogenic source-emissions in the wintertime continental outflow, concentrations of K^+ , Ca^{2+}

and SO_4^{2-} were corrected for the contribution from sea salt aerosols (if any) using the Na^+ levels in the TSP according to Keene et al. (1986). Overall, we observed different latitudinal gradients for the measured chemical constituents (Figure 2).

Of the WSIS, Na^+ , Mg^{2+} and Cl^- showed higher concentrations at the central Arabian Sea as compared to its south and northern coastal parts. In contrast, the anthropogenic WSIS (*i.e.*, NH_4^+ , non-sea-salt or nss- K^+ , and nss- SO_4^{2-}) loadings are higher in the TSP samples collected over the southern than the northern Arabian Sea. Emissions from biomass burning and coal combustion contribute to high levels of water-soluble K^+ and SO_4^{2-} , respectively in the continental outflows (Bikkina and Sarin, 2014). The estimated nss- SO_4^{2-} and nss- K^+ accounted to 82-90% and 63-95% of mass concentrations of SO_4^{2-} ($2.5 - 15.8 \mu\text{g m}^{-3}$) and K^+ ($0.3 - 1.5 \mu\text{g m}^{-3}$), respectively, over the Arabian Sea during the winter which indicates dominant contribution from continental sources. The higher loadings of nss- K^+ and nss- SO_4^{2-} over 5-15 °N latitudes indicate a strong influence from the continental pollution from southern India. In contrast, the concentration of other WSIS (nss- Ca^{2+} and NO_3^-) were higher in the TSP collected in the northern than the southern Arabian Sea. Several studies demonstrated that water-soluble Ca^{2+} in the continental outflows mainly come from calcium carbonate-rich mineral dust from the Thar Desert in Rajasthan and other nearby desert regions bordering the Indian subcontinent (Rastogi and Sarin, 2006; Kumar and Sarin, 2009). Therefore, it is likely that high loadings of nss- Ca^{2+} in the TSP samples collected over 20 – 24 °N latitudes could be due to their proximity to these deserts. However, similar latitudinal variability of NO_3^- with nss- Ca^{2+} could be due to heterogeneous uptake of HNO_3 by mineral dust, which is also evidenced by the co-occurrence of nss- Ca^{2+} and NO_3^- in coarse mode particles (Kumar et al., 2008a; Bikkina et al., 2011; Cruz et al., 2019).

The radiative forcing of aerosols over a geographical domain is somewhat governed by the atmospheric loadings of carbonaceous components (EC, and OC). Therefore, we have examined the latitudinal variability of mass concentrations OC and EC over the Arabian Sea (Figure 2i-j). The variability of carbonaceous components here is similar to that of nss- Ca^{2+} , whose concentrations peaked in the northern latitudes and decreased significantly towards the southern Arabian Sea. The concentrations of EC ($1.4 \pm 0.5 \mu\text{g m}^{-3}$) and OC ($6.7 \pm 3.3 \mu\text{g m}^{-3}$) over the Arabian Sea are lower than the previously reported values (EC: $2.2 \pm 0.9 \mu\text{g m}^{-3}$; OC: $9.8 \pm 3.8 \mu\text{g m}^{-3}$) by Kumar et al. (2012), however, somewhat higher than those (EC: $0.9 \pm 0.1 \mu\text{g m}^{-3}$; OC: $3.0 \pm 0.5 \mu\text{g m}^{-3}$) documented by Aswini et al. (2020). Furthermore, the EC and OC concentrations reported over the Arabian Sea are also comparable to those reported over the Bay of Bengal during winter (EC: $1.8 \pm 1.4 \mu\text{g m}^{-3}$; OC: $6.3 \pm 5.2 \mu\text{g m}^{-3}$; (Bikkina and Sarin, 2013)). This comparison provides an idea about the large inter-

annual variability associated with abundances of carbonaceous components in the continental outflows. Some of the environmental factors influencing this inter-annual variability include wind speed and emission strength of pollutants as well as influence from local (*i.e.*, from southern India) versus regional transport (*i.e.*, from the IGP).

The proportions of WSOC and WIOC also provide insights into the ambient photochemical processing of organic aerosols during transport (Saxena and Hildemann, 1996; Sullivan and Weber, 2006; Favez et al., 2008). Both WSOC and WIOC exhibited pronounced latitudinal variability and their mass concentrations varied from 1.5 to 7.8 $\mu\text{g m}^{-3}$ ($3.7\pm 4.5 \mu\text{g m}^{-3}$) and 0.8 to 11.0 $\mu\text{g m}^{-3}$ ($2.9\pm 2.4 \mu\text{g m}^{-3}$), respectively. In particular, we observed higher loadings of WSOC and WIOC over the northern latitudes and decreased towards southern latitudes (Figure 2k-l). Here, the remarkable similarity in the latitudinal variability of WSOC with OC and EC further suggesting their less modification due to dilution effect during transport and, perhaps, governed largely by the source-emissions. Besides, the WSOC levels from this study over the Arabian Sea are comparable to those reported other winter cruises in the Arabian Sea ($8.6\pm 2.9 \mu\text{g m}^{-3}$; (Kumar et al., 2012); $2.2\pm 0.8 \mu\text{g m}^{-3}$; (Aswini et al., 2020)), the Bay of Bengal (Nov' 2008: $6.7\pm 3.9 \mu\text{g m}^{-3}$; Dec' 2008-Jan' 2009: $5.5\pm 3.1 \mu\text{g m}^{-3}$ (Bikkina and Sarin, 2013)).

3.2. Impact of biological activity-MSA and biogenic SO_4^{2-} levels

Methanesulfonic acid (MSA) is an atmospheric oxidation product of a biogenic volatile organic compound, dimethyl sulfide (DMS), emitted from the ocean surface (Hatakeyama and Akimoto, 1983; Bates et al., 1992). Here, the DMS is in turn produced from the enzymatic cleavage of a phytoplankton exudate, dimethylsulfoniopropionate (Cantoni and Anderson, 1956). In addition to MSA, DMS oxidation in the marine atmosphere is also a source of nss-SO_4^{2-} (Hatakeyama and Akimoto, 1983; Hatakeyama et al., 1985). As a result, caution should be maintained while interpreting the non-sea-salt or nss-SO_4^{2-} concentrations over productive oceanic regions (*e.g.*, here Arabian Sea) influenced by anthropogenic emissions. Johansen et al. (1999) reported that nss-SO_4^{2-} levels over the Arabian Sea are contributed by the DMS oxidation in the marine atmosphere plus long-range transport of anthropogenic emissions.

$$\text{nss-SO}_4^{2-} = \text{anthropogenic SO}_4^{2-} + \text{biogenic SO}_4^{2-} \quad (1)$$

The likely presence of the continental sulphur species associated with anthropogenic emissions can be traced by the similarity in the latitudinal variability of nss-SO_4^{2-} and NH_4^+ . Because of the predominant oceanic origin of precursor DMS, the distributions of MSA levels in the marine atmosphere often discussed in terms of the biological activity in the underlying surface waters and

the resultant sea-to-air efflux (Saltzman et al., 1986; Mihalopoulos et al., 1992; Johansen et al., 2000; Chen et al., 2012). The biogenic SO_4^{2-} (*i.e.*, formed via DMS oxidation) contributes significantly to nss-SO_4^{2-} levels in marine aerosols. Therefore, we can use the MSA concentrations in TSP samples to assess the contribution of biogenic SO_4^{2-} to total nss-SO_4^{2-} over the Arabian Sea using the following mathematical expression.

$$\text{biogenic } \text{SO}_4^{2-} = [\text{MSA}]_{\text{aero}} \times (\text{nss-SO}_4^{2-}/\text{MSA})_{\text{bio}} \quad (2)$$

Here $[\text{MSA}]_{\text{aero}}$ refers to the concentration of MSA and the $(\text{nss-SO}_4^{2-}/\text{MSA})_{\text{bio}}$ corresponds to the mass ratio of these two chemical species in marine aerosols influenced mostly by the oceanic biological activity (Zhang et al., 2013). Numerous researchers have observed a significant linear relationship between MSA and nss-SO_4^{2-} over the remote Pacific Ocean Island. Savoie and Prospero (1989) have carried out long-term measurements at Samoa, an island with less influence from the continental outflows, and suggested to use a value of 18-20 for the mass ratio of $(\text{nss-SO}_4^{2-}/\text{MSA})_{\text{bio}}$ to constrain the biogenic SO_4^{2-} contribution in the tropical marine aerosols (Savoie and Prospero, 1989). However, Johansen and Hoffmann (2004) have used their earlier proposed temperature dependence relationship of biogenic $\text{SO}_4^{2-}/\text{MSA}$ ratio by Johansen et al. (1999) and the ambient temperature of 25.3 °C to predict the source-specific signature (~9-10) for the marine aerosols from the Arabian Sea. Using the same relationship and the observed mean ambient temperature during SS379 cruise (~27.3 °C), we predicted the biogenic $\text{SO}_4^{2-}/\text{MSA}$ ratio as 14 over the Arabian Sea.

We have, therefore, examined the latitudinal variability of MSA concentrations over the Arabian Sea during the SS379 winter cruise (Figure 3a). The MSA concentrations over the Arabian Sea are higher over northern latitudes (14-23 °N) than those over the low latitudes (8 -14 °N). Here, the observed higher abundances of MSA over these low latitudes are consistent with an increase in biological activity in the surface waters reported off the coast of southeastern Arabian Sea. Using the predicted $(\text{nss-SO}_4^{2-}/\text{MSA})_{\text{bio}}$ ratio (~14) and the concentration of MSA, we have, thus, estimated the atmospheric levels of biogenic SO_4^{2-} (Figure 3b) and its contribution to total nss-SO_4^{2-} (Figure 3c) over the Arabian Sea. Overall, the concentration of biogenic SO_4^{2-} over the Arabian Sea during SS379 cruise varied from 0.23 $\mu\text{g m}^{-3}$ to 1.64 $\mu\text{g m}^{-3}$ ($0.74 \pm 0.42 \mu\text{g m}^{-3}$). These atmospheric loadings of biogenic SO_4^{2-} , thus, contributes to ~2.3-22% ($17 \pm 6\%$) over the Arabian Sea during the study period. Our estimated contribution of biogenic SO_4^{2-} to nss-SO_4^{2-} in TSP sampled from the offshore waters of the east coast of Arabian Sea is somewhat higher than those observed for the marine aerosols collected over the central and west coast (~6%) of the Arabian Sea (Johansen and Hoffmann, 2004).

3.3. Charge balance and relative abundance of inorganic ions

The ion balance, representing the comparison of an equivalent concentration of cations (Σ^+) and anions (Σ^-), provide information on the overall relative dominance of water-soluble alkaline versus acidic species in ambient aerosols. We found that the regression slope value of Σ^- versus Σ^+ (slope = 1.12; $R^2 = 0.90$; $p < 0.05$) is more than unity, suggesting anion deficit in TSP samples collected during SS379 cruise. Here, the anion deficit could be due to a lack of consideration of contribution from missing components (*e.g.*, HCO_3^- , organic acids). The WSIS concentration varied from 12.9-51.3% ($32.3 \pm 10.6\%$) of TSP mass over the Arabian Sea during our winter cruise. These WSIS levels are somewhat comparable with the continental outflow samples collected from the Bay of Bengal ($45 \pm 9\%$; (Bikkina and Sarin, 2014)), but significantly higher than those observed over the urban sites in India (Hisar: $20 \pm 7\%$ (Rengarajan et al., 2007); Manora peak, Nainital: $15 \pm 3\%$ (Rengarajan et al., 2007); Kanpur: $16 \pm 2\%$; (Ram and Sarin, 2011); Kharagpur: $31 \pm 14\%$; (Bikkina and Sarin, 2014)) and China (Xian: 24%; (Xiao and Liu, 2004); Shanghai: 26%; (Wang et al., 2006)).

The latitudinal variability of relative abundances of individual WSIS in their total mass concentration ($19.1 \pm 5.7 \mu\text{g m}^{-3}$) is revealed by and large with the predominance of SO_4^{2-} ($42.4 \pm 9.7\%$) followed by Na^+ ($14.4 \pm 5.5\%$), Cl^- ($10.3 \pm 4.4\%$), NH_4^+ ($9.2 \pm 5.4\%$) and NO_3^- ($10.9 \pm 4.5\%$) in the TSP collected over the Arabian Sea during the winter (Figure 4a). All other components (Ca^{2+} : $5.1 \pm 4.3\%$; K^+ : $2.9 \pm 1.1\%$; Mg^{2+} : $1.6 \pm 1.1\%$) contributed to $\sim 10\%$ of WSIS mass (Figure 3a). Given the predominance of SO_4^{2-} , we further apportioned this fraction into seasalt SO_4^{2-} , biogenic SO_4^{2-} and anthropogenic SO_4^{2-} . The latitudinal variability of these three fractions in total SO_4^{2-} in TSP samples revealed the predominance of anthropogenic sources over the Arabian Sea (Figure 4b). Here, the latitudinal variability of WSIS concentrations during the SS379 cruise along with the backward air mass trajectories (dashed lines) and MODIS firecount data (orange dots) was also shown as an insert in Figure 4a.

Most of the trajectories for the TSP samples intercepting the firespots over the IGP and southern India. The IGP is a hotspot of SO_2 emissions and, hence, its oxidation product, anthropogenic SO_4^{2-} from the coal fired power plants. Therefore, the large abundance of SO_4^{2-} (or anthropogenic SO_4^{2-}) over the Arabian Sea could be due to long-range transport of coal fired power plant emissions. Furthermore, Overall, anthropogenic ions ($\text{WSIS}_{\text{anth}}$: $\text{anthropogenicSO}_4^{2-} + \text{NO}_3^- + \text{NH}_4^+ + \text{nss-K}^+$) contributed to $\sim 61 \pm 17\%$ of WSIS load. In contrast, anthropogenic ions account for 89% (anthropogenic- SO_4^{2-} : 62%; NH_4^+ : 19%, NO_3^- : 5%; nss-K^+ : 3%) of total mass concentration of WSIS (av. $23.3 \mu\text{g m}^{-3}$) in PM_{10} collected over the entire Bay of Bengal during winter 2008 (27

December 2008-26 January 2009) (Bikkina and Sarin, 2012; Bikkina and Sarin, 2013). This preliminary comparison, although with the limited datasets, suggests that the Arabian Sea is relatively less influenced by the pollution sources from the IGP as compared to the Bay of Bengal. However, more long-term measurements are needed to better constrain the relative impact of anthropogenic sources over both marine basins of the northern Indian Ocean.

3.4. Source apportionment

To evaluate the possible sources of TSP, chemical composition data collected over the Arabian Sea were subjected to multiple linear regression (MLR) analysis (Figure 5). The MLR matrix among the measured WSIS revealed strong correlations among Na^+ , Cl^- and Mg^{2+} , suggesting their origin from sea salt aerosols. Likewise, SO_4^{2-} and NH_4^+ are strongly correlated, suggesting their formation as ammonium sulphate or ammonium bisulphate in the continental outflow to the Arabian Sea. The slope of the linear regression provides information on the nature and processing of marine aerosols. The slope of the linear regression between the equivalent mass concentration of NH_4^+ and nss-SO_4^{2-} is 0.88 (*i.e.*, <1 ; Figure 6a), indicating the presence of excess acid available for other chemical reactions in the marine atmospheric boundary layer over the Arabian Sea. In such a case, one would expect that this excess inorganic acidic species likely react with other major alkaline aerosol species over the Arabian Sea.

The reactive heterogeneous uptake of anthropogenic sulfuric acid, nitric acid and other organic acids by seasalt aerosols could knock off Cl^- as a hydrochloric acid vapour causing a phenomenon called “chloride depletion” (Braun et al., 2017; Song et al., 2018; AzadiAghdam et al., 2019). The possible sea salt reaction with acidic species in the continental outflow can be easily traced by validating the strength and slopes of the linear regressions of Na^+ with Cl^- and Mg^{2+} in marine aerosols (Figure 5b,c). Though both Cl^- and Mg^{2+} exhibited strong linear relationships with Na^+ in TSP, the slope of the linear regression between Na^+ and Cl^- is well below (0.36) the weight ratio of seawater (1.8; Figure 6b). In contrast, the regression slope of Na^+ with Mg^{2+} is similar (0.13) to that of their weight ratio in seawater (0.12; Figure 6c). These observations clearly emphasize that Cl^- from sea salt aerosols (*i.e.*, represented by NaCl as its contribution is $>90\%$ by mass) is expelled by the reactive uptake of acidic species in the continental outflow to the Arabian Sea in winter. It is noteworthy that when an excess equivalent amount of nss-SO_4^{2-} is added to that of Cl^- concentrations, the regression slope with Na^+ is approaching the seawater line (Figure 6d). Therefore, it is reasonable to argue that the presence of excess of anthropogenic SO_4^{2-} is responsible for the Cl^- -depletion over the Arabian Sea in winter.

The estimated Cl-depletion values from this study are also comparable to those earlier two cruises from the Arabian Sea and Bay of Bengal (Kumar et al. (2012), indicating a likely common behaviour of the continental outflows to the northern Indian Ocean. However, anions of organic dicarboxylic acids (such as oxalate, malonate and succinate) can also account for the minor contribution to the depletion of chlorine in the marine aerosols over the Arabian Sea, which cannot be overlooked. This becomes an obvious reason for air spending a long time over the continent as reported by Kerminen et al. (1998) near the Arctic Ocean. Due to the lack of concentration data of these organic compounds, our discussion is mainly limited to the role of major inorganic ions on the chloride-depletion from the seasalt aerosols.

The strong linear relationship between OC and EC in the TSP is observed over the Arabian Sea (Figure 7a) with a slope value of ~ 4.0 ($R^2 = 0.80$; p-value < 0.05). One TSP sample (SS379_TSP#16; collected on 22 December 2018) was excluded for the regression for which back trajectories originate from the northern Bay of Bengal. This observation suggested that carbonaceous aerosols could have origins from both fossil fuel combustion and biomass burning emissions. Furthermore, the robustness and regression slope between WSOC and OC are investigated to assess the relative importance of these two source-emissions as fossil fuel combustion contributes very less to the atmospheric abundances of WSOC as compared to biomass burning. WSOC levels are strongly correlated with OC concentrations over the Arabian Sea during the present cruise (Figure 7b), demonstrating a likely predominance of biomass burning emissions. This conclusion is further supported by 7-day isentropic backward air mass trajectory and MODIS fire count data for the study period (see inset in Figure 4a). Similarly, a significant linear relationship was observed between WIOC and EC with a regression slope value of ~ 1.8 (Figure 7c), being consistent with the value from PM₁₀ samples over the Bay of Bengal, which is influenced by the IGP-outflow in winter (Bikkina and Sarin, 2012). This study thus emphasizes the applicability of OC and EC as robust tracers for assessing the impact of the IGP over the northern Indian Ocean during the continental outflow.

3.5. Diagnostic mass ratios

Several diagnostic mass ratios of carbonaceous and inorganic components (*i.e.*, listed in Table 1) provide additional information about the impact of various pollution sources over the Arabian Sea. For instance, equivalent mass ratios of NH₄⁺ to nss-SO₄²⁻ in most of the TSP samples are lower than unity (Figure 8), implying the presence of acidic marine aerosols over the Arabian Sea during the winter period. Besides, the equivalent mass ratios of NH₄⁺/nss-SO₄²⁻ from this study are comparable to those documented over the Bay of Bengal (Bikkina and Sarin, 2014) during the winter

period but slightly less than those reported over the Arabian Sea (Kumar et al. (2012)). This comparison represents broad inorganic acidity levels in the continental outflows during the winter period. Kumar et al. (2012) reported the equivalent mass ratios of $\text{NH}_4^+/\text{nss-SO}_4^{2-}$ as 0.70 during SS259 (December 2007), whereas Aswini et al. (2020) reported an average of 0.77 ± 0.18 during January-February 2018. Irrespective of the time intervals of the sampling periods, all these marine aerosols indicate that there is an excess anthropogenic non-sea-salt SO_4^{2-} over NH_4^+ , suggesting ammonium poor or acid-rich environment.

The mass ratio of NO_3^- to SO_4^{2-} over a geographical location provides information on the relative importance of vehicular emissions versus coal fired power plants to atmospheric aerosols (Huebert et al., 1988). This is mainly because automobile emissions are the major source of NO_x , which is oxidized in the atmosphere to form NO_3^- , whereas the coal fired power plants dominant SO_2 emissions and, hence, SO_4^{2-} from the continental sources. $\text{NO}_3^-/\text{anthropogenic-SO}_4^{2-}$ ratio in TSP over the Arabian Sea is much lower than unity (0.09-0.65; av. 0.31 ± 0.19). This observation suggesting that stationary sources (*i.e.*, from coal fired power plants) are more important contributors to the airborne particulate matter than mobile sources (*i.e.*, vehicular emissions) in the South Asian outflow sampled over the Arabian Sea during the winter season. Additionally, the $\text{NO}_3^-/\text{anthropogenic-SO}_4^{2-}$ ratios from this study are similar to those reported over the Bay of Bengal (0.01 – 0.43) and the urban sites in South Asia (Hisar: 1.1 ± 0.4 (Rengarajan et al., 2007); Manora peak, Nainital: 0.23 ± 0.18 (Rengarajan et al., 2007)); Kanpur: 0.52 ± 0.20 (Ram and Sarin, 2011); Kharagpur: 0.20 ((Bikkina and Sarin, 2014)) and East Asia (Guiyang: 0.13; (Xiao and Liu, 2004); Shanghai: 0.83 ± 0.40 ((Wang et al., 2006); Beijing: 0.58(Yao et al., 2002); Beijing: 0.3-0.5 (Huebert et al., 1988)).

The $\text{nss-K}^+/\text{nss-Ca}^{2+}$ and $\text{nss-SO}_4^{2-}/\text{nss-Ca}^{2+}$ are also useful tracers for assessing the relative influence of biomass burning and coal combustion over mineral dust. This is because nss-K^+ and nss-SO_4^{2-} are more abundant in emissions from biomass burning and coal combustion, respectively, whereas nss-Ca^{2+} is regarded as a tracer for dust input (Rastogi and Sarin, 2006; Bikkina et al., 2014). Both these mass ratios showed higher values in the southern Arabian Sea due to distant locations sampled away from the dust source regions in the north and, hence, a decrease in the contribution of mineral dust. Besides, we found high concentrations of nss-K^+ and nss-SO_4^{2-} in these southernmost samples because of the influence from biomass burning emissions and coal combustion over the IGP (supported by backward air mass trajectories and firecount data).

Another set of proxies that can be examined for assessing the relative influence of carbonaceous aerosols from biomass burning and coal combustion are OC/EC, nss-K⁺/EC, nss-K⁺/OC and nss-SO₄²⁻/EC. The mass ratios of OC/EC from fossil fuel combustion (2-4) are comparatively lower than those of biomass burning emissions (4-12). OC/EC ratios over the Arabian Sea (2.5-10.5; av. 4.9±1.8) indicate the impact of biomass burning emissions in the northern and southern Arabian Sea during the winter period. This observation is further corroborated by the mass ratios of nss-K⁺/EC (0.45±0.26) and nss-K⁺/OC (0.10±0.07), which are quite similar to those documented for the open burning of postharvest crop-residues in the IGP (0.79±0.22 and 0.07±0.04, respectively) (Rastogi et al., 2015). Besides this, the nss-K⁺/EC and nss-K⁺/OC from this study are comparable to those observed for the IGP-outflow to the Bay of Bengal (0.49±0.22 and 0.07±0.04) (Bikkina and Sarin, 2014) but somewhat lower than those for the intense biomass burning emissions in the Amazon basin (0.90±0.32 and 0.04±0.01) (Kundu et al., 2010).

The nss-SO₄²⁻/EC ratios can be used to decipher the relative influence of nss-SO₄²⁻ and EC from coal combustion over other anthropogenic sources. Atmospheric SO₄²⁻ is an oxidation product of gaseous SO₂. For the Indian subcontinent, coal-fired thermal power plants generate electricity, which is the major source of ambient SO₂ but also emit substantial quantities of EC. In contrast, both vehicular emissions and biomass burning contribute substantially to high levels of EC with low SO₂. Because of the short tropospheric lifetime (<2h to 2 days; (Pandis and Seinfeld, 2006; Lee et al., 2011; Mallik et al., 2013)), SO₂ is rapidly converted to SO₄²⁻ aerosols and, hence, the mass ratio of SO₄²⁻/EC can be used as a pseudo-tracer for the continental outflows like K⁺/EC. Accordingly, we compared the nss-SO₄²⁻/EC ratios from the Arabian Sea (6.8±3.0) with the estimates derived from biomass burning (1.4±0.9;(Kundu et al., 2010); 2.6±0.4(Rajput et al., 2014b), 2.8±1.6(Rastogi et al., 2015)) and coal-fired power plant emissions (3.9±2.1) in the IGP and the IGP-outflow to the Bay of Bengal (6.2±3.6) (Bikkina and Sarin, 2012). This comparison strengthens the influence of coal combustion in the IGP than other anthropogenic sources over the coastal Arabian Sea.

The WSOC/OC ratio is also a tracer to distinguish the relative importance of fossil-fuel combustion versus biomass burning emissions. Fossil fuel combustion contributes to lesser WSOC of OC (Aggarwal et al., 2013) than biomass burning emissions and, consequently, the latter source-emissions are characterized by higher WSOC/OC (0.65±0.14, (Kundu et al., 2010)). In this study, the observed WSOC/OC ratios over the Arabian Sea (0.59±0.12) are comparable to those from biomass burning emissions in the IGP (0.52±0.16 (Bikkina and Sarin, 2014); 0.52±0.06 (Rajput et al., 2014a)) but lower than those reported for other marginal seas (Bohai Sea: 0.71±0.13%, Yellow Sea: 0.66±0.13%(Ding et al., 2019)). Apart from the source-emissions, ageing effect (oxidation) and/or

secondary formation of organic aerosols, both these processes contribute to an overall increase in WSOC/OC ratios (Bikkina and Sarin, 2014).

Several factors including solar radiation, ambient relative humidity and aerosol liquid water content (ALWC), including processing can affect the WSOC/OC ratios (Youn et al., 2013; Xiang et al., 2017). Therefore, we looked for any significant linear relationship between WSOC/OC and these parameters over the Arabian Sea. The latitudinal variability and relationship of downwind solar flux values obtained from the HYSPLIT-based backward trajectories were examined for understanding their effect on atmospheric abundances of WSOC and WSOC/OC. We estimated the ALWC using the meteorological parameters and the concentrations of WSIS in the ISORROPIA-II (Fountoukis and Nenes, 2007), a thermodynamic equilibrium partition model, for the TSP samples collected over the Arabian Sea. No significant linear relationship was observed between the estimated ALWC and WSOC over the Arabian Sea (Figure S1). This observation suggests a less influence of aqueous phase chemical reactions to the formation of WSOC over the Arabian Sea. One possible reason could be because of the more alkaline tendency of TSP samples (*i.e.*, more dust influence) over the Arabian Sea. In contrast, the observations from the Bay of Bengal revealed that aerosol acidity controls the abundances of WSOC in the winter season (Bikkina et al., 2017).

In this study, WSOC is inversely correlated with both ambient relative humidity (RH) over the Arabian Sea during the SS379 cruise (Figure S2a). Although rather weak, such an inverse trend also exists between WSOC concentrations and ambient temperature over the Arabian Sea (Figure S2b). From Figure S1a-b, it is clear that the data scattered into two clusters in which TSP samples with higher WSOC and OC levels are, in particular, associated with lower ambient RH (40-50%) and temperature. This feature could be because of the latitudinal dependencies of ambient RH and temperature as well as the transport influence of carbonaceous components from the nearby and distant pollution source-emissions. In other words, the cold (4-24°C) and dry continental air masses (RH: 40-60%) over northern India (*e.g.*, over IGP) in winter season usually characterized by higher atmospheric abundances of WSOC and OC. This is mostly due to entrainment of pollutants near to ground because of the prevailing shallow atmospheric boundary layer (<700 m) and more stagnant weather conditions. In contrast, higher ambient RH and temperature for the TSP samples collected over low latitudes (*i.e.*, moving towards the equator) (5-13 °N) along with lower loadings of WSOC and OC could be due to an increase in distance from the source emissions. Likewise, we observe a good linear relationship between WIOC and EC over the Arabian Sea and the ratio of WIOC/EC (2.2 ± 1.5) is somewhat comparable to those reported for the IGP-outflow (3.7 ± 1.5) (Bikkina and

Sarin, 2014). All these interpretations are supported by 7-day isentropic backward air mass trajectories and MODIS fire count data originated from the IGP.

3.6. Estimation of secondary organic carbon (SOC)

Traditionally, SOC fraction is estimated by the EC-tracer method, which can be best described by the following mathematical equations.

$$\text{Primary organic carbon, [POC]} = (\text{OC/EC})_{\text{primary}} \times [\text{EC}] \quad (1)$$

$$\text{Secondary organic carbon, [SOC]} = [\text{OC}] - [\text{POC}] \quad (2)$$

This approach works well because EC is solely originated from the primary source-emissions (*e.g.* fossil fuel combustion, biomass burning). Several ways adopted to constrain the possible primary OC/EC ratio. Some of them include the minimum or the lower 10 percentile of OC/EC ratio as the representative primary source-emission value observed over a study site. Generally, OC/EC ratios from the fossil fuel combustion are in between 2 and 4 whereas biomass burning emissions are in between 4 and 10 depending on the phase (*i.e.*, smouldering vs. flaming) and type of biomass (*e.g.* wood vs. crop). Therefore, if the major source of carbonaceous aerosols is fossil fuel combustion over the sampling site, then the minimum or lower 10-percentile OC/EC ratio is expected for the primary source-emissions. However, this approach of using minimum or lower 10-percentile OC/EC could lead to overestimation of SOC, if the biomass burning dominates or contributes equally to fossil fuel combustion sources. As a result, the SOC estimates using minimum or the lower 10-percentile of OC/EC ratio in the EC-tracer method causes large uncertainties. Alternatively, Millet et al. (2005) first proposed to use an unambiguous approach based on the minimum R-squared (MRS) method to estimate the primary OC/EC ratio from the source emissions. This method works on the principle by minimizing the coefficient of determination (R^2) of the linear regression between estimated SOC and EC by simultaneously varying the initial primary OC/EC ratios over a wide range.

In this study, we estimated the primary OC/EC ratio from the source emissions method (MRS) based on the Igor program developed and efficiently demonstrated by Wu and Yu (2016) for determining the ambient SOC levels over Chinese megacities (Zhang et al., 2019). For the present dataset, the estimated primary OC/EC ratio based on the MRS method was 4.2 (Figure 9). We also compared the estimated SOC concentrations using the MRS method with two other traditional approaches that use minimum and lower 10-percentile value of OC/EC ratios from the present data (Figure 10). Because of higher primary OC/EC ratio obtained from the MRS method, 35% of the TSP samples yielded negative values, unlike the SOC estimates based on the minimum OC/EC ratio

(*i.e.*, this method retained 94% of the data). Overall, the estimated SOC concentrations by the MRS method (0.91-4.53 $\mu\text{g m}^{-3}$) account for 7-61% (av. 23%) of OC and 0.7-11% (~3%) of TSP. In contrast, the estimated SOC levels based on the minimum and 10-percentile OC/EC ratio provided a much higher contribution towards OC load (20-76% and 5-67%, respectively). Furthermore, a remarkable similarity was found for the ranges and median values of SOC relative to OC from the MRS method (24%) and lower 10-percentile based method (23%).

3.7. Mass closure

To explain the contributions of measured chemical constituents to TSP mass, we attempted to assess the mass closure by accounting for the total carbonaceous aerosol load (TCA), major anthropogenic water-soluble inorganic species (WSIS_{anth}), seasalt and the remaining unidentified fraction. Here, the TCA includes both contributions from particulate organic matter (OM) and EC. Particulate organic matter over a source region can be well represented by the mass concentration of OC. However, it is not the case for remote locations because OC is secondarily produced by the oxidative reactions during long-range transport in which some carbon atoms are replaced by heteroatoms (*e.g.*, O, N, and S). Hence, we need to scale up the OC load by a factor based on the typical composition of organic compounds observed over the distant locations. In general, anthropogenic source-emissions contain relatively simple hydrocarbon mixture and less hetero-group containing estimated OM/OC ratios are about 1.4-1.6 and those observed for remote regions are about 1.8-2.1 (Turpin and Lim, 2001). By accounting for all the major components, except organic matter concentration in TSP mass, Bikkina and Sarin (2014) deduced a conversion factor of 2.0 for the IGP-outflow. This is also somewhat close to that estimated (*i.e.*, 1.9) for the IGP (Rajput et al., 2014b). Therefore, we used a conversion factor of 2.0 to assess the OM load in TSP. Likewise, WSIS_{anth} mass concentration is estimated as the sum of atmospheric loadings of NH_4^+ , nss-K^+ , NO_3^- and nss-SO_4^{2-} . Seasalt is estimated by using the Na^+ concentration in TSP times the weight ratio of this major element to the salinity of seawater (*i.e.*, $\text{Na}^+/\text{Salinity} \approx 3.2$). The unaccounted fraction contains both contributions from mineral dust and particulate-bound water content (*aka* aerosol liquid water content: ALWC).

Kumar et al. (2012) estimated contribution of mineral dust over the AS (~20-50%) using Al concentration in TSP and using their abundance percentage in the upper continental crust (~8.2% of dust is Al). Therefore, we presumed that the remaining unaccounted fraction is largely composed of mineral dust. Using this approach, we could approximate the percentage contribution of dust to TSP over the AS to be $55 \pm 10\%$. However, a substantial contribution of TSP mass was associated with the particulate bound water content (*i.e.*, 10% (Bikkina and Sarin, 2014)) and, hence, the likely estimate

for dust contribution is about 45%. The latitudinal variability of all these chemical components contributed to TSP mass are depicted in Figure 11. Furthermore, the latitudinal variability of TSP mass concentrations along the cruise track of SS379 cruise was shown as an inset in Figure 11.

Of the WSIS, anthropogenic ions including nss-SO_4^{2-} (6.6-29.2%), NO_3^- (1.0-7.7%), NH_4^+ (0.5-8.0%) and nss-K^+ (0.4-1.8%) mostly contribute to mass concentration of TSP over the AS. Overall, the contribution of $\text{WSIS}_{\text{anth}}$ (*i.e.*, $\text{nss-SO}_4^{2-} + \text{NO}_3^- + \text{NH}_4^+ + \text{nss-K}^+$) averages $20.9 \pm 8.8\%$ of TSP load over the Arabian Sea, which is higher than those estimated for the wintertime PM_{10} sampled over the Bay of Bengal ($34.7 \pm 7.1\%$) (Bikkina and Sarin, 2012). Likewise, OM accounts for 6.0-48.5% ($21.4 \pm 10.1\%$) of TSP over the Arabian Sea, which is consistent with previous measurements from the AS ($15.7 \pm 6.1\%$ (Kumar et al., 2012); $\sim 21\%$ (Aswini et al., 2020)) and the Bay of Bengal ($\sim 25.0 \pm 9.6\%$; estimated from PM_{10} data (Bikkina and Sarin, 2014)). Besides this, EC contributes to only $2.3 \pm 1.1\%$ (0.5-5.5%) of TSP mass over the Arabian Sea, which is similar to those from the northern Indian Ocean (3.2% (Aswini et al., 2020); $2.9 \pm 1.5\%$ (Kumar et al., 2012); $4.2 \pm 1.5\%$ (Bikkina and Sarin, 2014)). However, the seasalt contribution is only $14.6 \pm 5.8\%$ to TSP over the Arabian Sea during the present study. This seasalt loading is comparable to that ($12.1 \pm 9.6\%$) reported over the Arabian Sea by Kumar et al. (2012) but higher than that ($4.2 \pm 1.5\%$) from the Bay of Bengal (Bikkina and Sarin, 2012).

The proportions of $\text{WSIS}_{\text{anth}}$, TCA and the remaining unaccounted fraction (*i.e.*, mostly dust) in TSP over the Arabian Sea can be compared with the available datasets from the Bay of Bengal and few receptor/source sites in the IGP during winter (Figure 12). It is implicit from Figure 12 that the fractional contribution of $\text{WSIS}_{\text{anth}}$ was clustering $\sim 10\text{-}35\%$ over the Arabian Sea and the IGP, while it is centring around $\sim 20\text{-}50\%$ over the Bay of Bengal. Likewise, the TCA mass fraction over the Arabian Sea (*i.e.*, mostly in between 10-30%) is somewhat lower than those observed over the Bay of Bengal (20-40%). This means that the Arabian Sea is less influenced by the anthropogenic pollution sources, as evident by the contributions from $\text{WSIS}_{\text{anth}}$ ($20.9 \pm 8.8\%$) and TCA ($23.7 \pm 11.0\%$), compared to the Bay of Bengal during the winter period. In contrast, the Arabian Sea receives more dust input (*i.e.*, most of data clustering $\sim 40\text{-}70\%$) compared to the Bay of Bengal (20-40%) in winter. Besides, we observed higher percentage fractions of TCA (30-60%) and mineral dust (20-60%) over the IGP during the winter period.

Similar to our results, Kumar et al. (2012) documented that the mass fractions of dust, TCA and $\text{WSIS}_{\text{anth}}$ average $\sim 34.4 \pm 8.5\%$, $23.4 \pm 2.1\%$, and $26.2 \pm 7.4\%$, respectively, in TSP samples over the Arabian Sea during another winter cruise conducted over a decade ago (SS256: 18-27 December 2007). Likewise, Aswini et al. (2020) reported that dust fraction dominates the TSP load in the air

masses over the Arabian Sea coming from northern India. Besides the dust, the WSIS_{anth} fraction from their study (~24%) also overlaps with our range but with a much less fraction of TCA over the Arabian Sea (7%) (Aswini et al., 2020). All these comparisons provided insights about the influence of continental outflow from the IGP over the Arabian Sea, which is weaker than the influence observed over the Bay of Bengal during winter.

4. Conclusions

The chemical composition of TSP samples collected over the Arabian Sea during the winter (December 2018) is characterized by the significant contribution from particulate organic matter (21±10%), EC(2.3±1.1%), anthropogenic water-soluble inorganic species (WSIS_{anth}: 20±9%), and the unidentified fraction (43±15%) including dust. Moreover, these features resemble those documented over the Arabian Sea during another winter cruise (December 2007) conducted 13 years ago (Kumar et al., 2012). Comparison of this composition with marine aerosols collected over the Bay of Bengal (Bikkina and Sarin, 2012) during the winter revealed that the Arabian Sea is less influenced by the anthropogenic pollution sources in terms of contribution from nss-SO₄²⁻ and particulate OM. Estimated SOC levels are as high as 63% of OC and 11% of the TSP mass. This observation suggests a significant and evolving nature of secondary organic aerosols during the impact of continental outflows on the marine atmosphere in the winter season. The diagnostic mass ratios of OC/EC, nss-K⁺/EC and WSOC/OC along with backward air mass trajectories and MODIS firecounts revealed the major contribution and impact of biomass burning emissions in the IGP and southern India on the abundances of organic aerosols over the Arabian Sea.

Acknowledgements

PB acknowledges the partial financial support from the DST-INSPIRE fellowship (DST/INSPIRE/04/2017/000324 dated 24/07/2017) and JASSO (Japan Student Service Organization) Follow up research fellowship 2019. PB is grateful to the Scientist-In-Charge and the Director of NIO for the support at the workplace. PB and VVSS are also thankful to the Ship Captain and crew for their support during the cruise. KK acknowledges the financial support from Japan Society for the Promotion of Science (JSPS) under the Joint Research Program-LEAD (JRPs-LEAD with DFG). Authors are thankful to the Chief Scientist Dr. GVM Gupta (CMLRE, Kochi) and participants onboard of SS379 for their help in the sampling. Authors thankfully acknowledge the NOAA Air Resources Laboratory for the access to the HYSPLIT model (<http://www.arl.noaa.gov/ready.html>). We also acknowledge NASA's Goddard Earth Sciences Data

and Information Services Center for providing access to MODIS aerosol optical depth and fire count data from the GES-DISC Interactive Online Visualization and analysis portal.

References

Aggarwal, S.G., Kawamura, K., Umarji, G.S., Tachibana, E., Patil, R.S., Gupta, P.K., 2013. Organic and inorganic markers and stable C-, N-isotopic compositions of tropical coastal aerosols from megacity Mumbai: sources of organic aerosols and atmospheric processing. *Atmos. Chem. Phys.* 13, 4667-4680.

Alam, K., Khan, R., Sorooshian, A., Blaschke, T., Bibi, S., Bibi, H., 2018. Analysis of Aerosol Optical Properties due to a Haze Episode in the Himalayan Foothills: Implications for Climate Forcing. *Aerosol and Air Quality Research* 18, 1331-1350.

Andreae, M.O., Ramanathan, V., 2013. Climate's dark forcings. *Science* 340, 280-281.

Aswini, A.R., Hegde, P., Aryasree, S., Girach, I.A., Nair, P.R., 2020. Continental outflow of anthropogenic aerosols over Arabian Sea and Indian Ocean during wintertime: ICARB-2018 campaign. *Science of The Total Environment* 712, 135214.

AzadiAghdam, M., Braun, R.A., Edwards, E.-L., Bañaga, P.A., Cruz, M.T., Betito, G., Cambaliza, M.O., Dadashazar, H., Lorenzo, G.R., Ma, L., MacDonald, A.B., Nguyen, P., Simpas, J.B., Stahl, C., Sorooshian, A., 2019. On the nature of sea salt aerosol at a coastal megacity: Insights from Manila, Philippines in Southeast Asia. *Atmospheric Environment* 216, 116922.

Balasubramanian, R., Karthikeyan, S., Potter, J., Wurl, O., Durville, C., 2013. Chemical characterization of aerosols in the equatorial atmosphere over the Indian Ocean. *Atmospheric Environment* 78, 268-276.

Bates, T.S., Calhoun, J.A., Quinn, P.K., 1992. Variations in the methanesulfonate to sulfate molar ratio in submicrometer marine aerosol particles over the south Pacific Ocean. *Journal of Geophysical Research: Atmospheres* 97, 9859-9865.

Bikkina, S., Andersson, A., Kirillova, E.N., Holmstrand, H., Tiwari, S., Srivastava, A.K., Bisht, D.S., Gustafsson, Ö., 2019a. Air quality in megacity Delhi affected by countryside biomass burning. *Nature Sustainability* 2, 200-205.

Bikkina, S., Haque, M.M., Sarin, M., Kawamura, K., 2019b. Tracing the relative significance of primary versus secondary organic aerosols from biomass burning plumes over Coastal Ocean using sugar compounds and stable carbon isotopes. *ACS Earth and Space Chemistry*.

Bikkina, S., Kawamura, K., Sarin, M., 2017. Secondary organic aerosol formation over Coastal Ocean: Inferences from atmospheric water-soluble low molecular weight organic compounds. *Environmental Science & Technology* 51, 4347-4357.

Bikkina, S., Sarin, M., 2012. Atmospheric pathways of phosphorous to the Bay of Bengal: contribution from anthropogenic sources and mineral dust. *Tellus B* 64.

Bikkina, S., Sarin, M.M., 2013. Light absorbing organic aerosols (brown carbon) over the tropical Indian Ocean: impact of biomass burning emissions. *Environmental research letters* 8, 044042.

- Bikkina, S., Sarin, M.M., 2014. PM_{2.5}, EC and OC in atmospheric outflow from the Indo-Gangetic Plain: Temporal variability and aerosol organic carbon-to-organic mass conversion factor. *The Science of the total environment* 487, 196.
- Bikkina, S., Sarin, M.M., Rengarajan, R., 2014. Atmospheric transport of mineral dust from the Indo-Gangetic Plain: Temporal variability, acid processing, and iron solubility. *Geochemistry, Geophysics, Geosystems* 15, 3226-3243.
- Bikkina, S., Sarin, M.M., Sarma, V.V.S.S., 2011. Atmospheric dry deposition of inorganic and organic nitrogen to the Bay of Bengal: Impact of continental outflow. *Marine Chemistry* 127, 170-179.
- Bond, T.C., Bergstrom, R.W., 2006. Light absorption by carbonaceous particles: An investigative review. *Aerosol Science and Technology* 40, 27-67.
- Braun, R.A., Dadashazar, H., MacDonald, A.B., Aldhaif, A.M., Maudlin, L.C., Crosbie, E., Aghdam, M.A., Hossein Mardi, A., Sorooshian, A., 2017. Impact of Wildfire Emissions on Chloride and Bromide Depletion in Marine Aerosol Particles. *Environmental Science & Technology* 51, 9013-9021.
- Burney, J., Ramanathan, V., 2014. Recent climate and air pollution impacts on Indian agriculture. *Proceedings of the National Academy of Sciences* 111, 16319-16324.
- Cantoni, G.á., Anderson, D.G., 1956. Enzymatic cleavage of dimethylpropiothetin by *Polysiphonia lanosa*. *Journal of Biological Chemistry* 222, 171-177.
- Chen, L., Wang, J., Gao, Y., Xu, G., Yang, X., Lin, Q., Zhang, Y., 2012. Latitudinal distributions of atmospheric MSA and MSA/nss-SO₄²⁻ ratios in summer over the high latitude regions of the Southern and Northern Hemispheres. *Journal of Geophysical Research: Atmospheres* 117.
- Cong, Z., Kang, S., Kawamura, K., Liu, B., Wan, X., Wang, Z., Gao, S., Fu, P., 2015. Carbonaceous aerosols on the south edge of the Tibetan Plateau: concentrations, seasonality and sources. *Atmospheric chemistry and physics* 15, 1573-1584.
- Cruz, M.T., Bañaga, P.A., Betito, G., Braun, R.A., Stahl, C., Aghdam, M.A., Cambaliza, M.O., Dadashazar, H., Hilario, M.R., Lorenzo, G.R., Ma, L., MacDonald, A.B., Pabroa, P.C., Yee, J.R., Simpas, J.B., Sorooshian, A., 2019. Size-resolved composition and morphology of particulate matter during the southwest monsoon in Metro Manila, Philippines. *Atmos. Chem. Phys.* 19, 10675-10696.
- Ding, X., Qi, J., Meng, X., 2019. Characteristics and sources of organic carbon in coastal and marine atmospheric particulates over East China. *Atmospheric Research* 228, 281-291.
- Draxler, R., Rolph, G., 2009. HYSPLIT (HYbrid Single-Particle Lagrangian Integrated Trajectory) Model access via NOAA ARL READY Website. NOAA Air Resources Laboratory, Silver Spring, MD, 2003.
- Fadnavis, S., Sabin, T.P., Roy, C., Rowlinson, M., Rap, A., Vernier, J.-P., Sioris, C.E., 2019. Elevated aerosol layer over South Asia worsens the Indian droughts. *Scientific Reports* 9, 10268.
- Favez, O., Sciare, J., Cachier, H., Alfaro, S.C., Abdelwahab, M.M., 2008. Significant formation of water-insoluble secondary organic aerosols in semi-arid urban environment. *Geophysical Research Letters* 35.

- Fountoukis, C., Nenes, A., 2007. ISORROPIA II: a computationally efficient thermodynamic equilibrium model for K^+ – Ca^{2+} – Mg^{2+} – NH_4^+ – Na^+ – SO_4^{2-} – NO_3^- – Cl^- – H_2O aerosols. *Atmos. Chem. Phys.* 7, 4639-4659.
- Gogoi, M.M., Babu, S.S., Moorthy, K.K., Bhuyan, P.K., Pathak, B., Subba, T., Chutia, L., Kundu, S.S., Bharali, C., Borgohain, A., Guha, A., De, B.K., Singh, B., Chin, M., 2017. Radiative effects of absorbing aerosols over northeastern India: Observations and model simulations. *Journal of Geophysical Research: Atmospheres* 122, 1132-1157.
- Gustafsson, Ö., Kruså, M., Zencak, Z., Sheesley, R.J., Granat, L., Engström, E., Praveen, P., Rao, P., Leck, C., Rodhe, H., 2009. Brown clouds over South Asia: biomass or fossil fuel combustion? *Science* 323, 495-498.
- Gustafsson, Ö., Ramanathan, V., 2016. Convergence on climate warming by black carbon aerosols. *Proceedings of the National Academy of Sciences* 113, 4243-4245.
- Hatakeyama, S., Akimoto, H., 1983. Reactions of hydroxyl radicals with methanethiol, dimethyl sulfide, and dimethyl disulfide in air. *The Journal of Physical Chemistry* 87, 2387-2395.
- Hatakeyama, S., Izumi, K., Akimoto, H., 1985. Yield of SO_2 and formation of aerosol in the photo-oxidation of DMS under atmospheric conditions. *Atmospheric Environment (1967)* 19, 135-141.
- Hu, B., Zhao, X., Liu, H., Liu, Z., Song, T., Wang, Y., Tang, L., Xia, X., Tang, G., Ji, D., Wen, T., Wang, L., Sun, Y., Xin, J., 2017. Quantification of the impact of aerosol on broadband solar radiation in North China. *Scientific Reports* 7, 44851.
- Huebert, B.J., Ming-Xing, W., Wei-Xiu, L., 1988. Atmospheric nitrate, sulfate, ammonium and calcium concentrations in China. *Tellus B* 40B, 260-269.
- Johansen, A.M., Hoffmann, M.R., 2004. Chemical characterization of ambient aerosol collected during the northeast monsoon season over the Arabian Sea: Anions and cations. *Journal of Geophysical Research: Atmospheres* 109.
- Johansen, A.M., Siefert, R.L., Hoffmann, M.R., 1999. Chemical characterization of ambient aerosol collected during the southwest monsoon and intermonsoon seasons over the Arabian Sea: Anions and cations. *Journal of Geophysical Research: Atmospheres* 104, 26325-26347.
- Johansen, A.M., Siefert, R.L., Hoffmann, M.R., 2000. Chemical composition of aerosols collected over the tropical North Atlantic Ocean. *Journal of Geophysical Research: Atmospheres* 105, 15277-15312.
- Keene, W.C., Pszenny, A.A., Galloway, J.N., Hawley, M.E., 1986. Sea-salt corrections and interpretation of constituent ratios in marine precipitation. *Journal of Geophysical Research: Atmospheres (1984–2012)* 91, 6647-6658.
- Kerminen, V.-M., Teinilä, K., Hillamo, R., Pakkanen, T., 1998. Substitution of chloride in sea-salt particles by inorganic and organic anions. *Journal of Aerosol Science* 29, 929-942.
- Krishna Moorthy, K., Suresh Babu, S., Manoj, M.R., Satheesh, S.K., 2013. Buildup of aerosols over the Indian Region. *Geophysical Research Letters* 40, 1011-1014.

- Kumar, A., Sarin, M.M., 2009. Mineral aerosols from western India: Temporal variability of coarse and fine atmospheric dust and elemental characteristics. *Atmospheric Environment* 43, 4005-4013.
- Kumar, A., Sarin, M.M., Sudheer, A.K., 2008a. Mineral and anthropogenic aerosols in Arabian Sea-atmospheric boundary layer: Sources and spatial variability. *Atmospheric Environment* 42, 5169-5181.
- Kumar, A., Sudheer, A., Sarin, M., 2008b. Chemical characteristics of aerosols in MABL of Bay of Bengal and Arabian Sea during spring inter-monsoon: a comparative study. *Journal of Earth System Science* 117, 325-332.
- Kumar, A., Sudheer, A.K., Goswami, V., Bhushan, R., 2012. Influence of continental outflow on aerosol chemical characteristics over the Arabian Sea during winter. *Atmospheric Environment* 50, 182-191.
- Kundu, S., Kawamura, K., Andreae, T.W., Hoffer, A., Andreae, M.O., 2010. Diurnal variation in the water-soluble inorganic ions, organic carbon and isotopic compositions of total carbon and nitrogen in biomass burning aerosols from the LBA-SMOCC campaign in Rondônia, Brazil. *Journal of Aerosol Science* 41, 118-133.
- Lau, K.M., Kim, M.K., Kim, K.M., 2006. Asian summer monsoon anomalies induced by aerosol direct forcing: the role of the Tibetan Plateau. *Climate Dynamics* 26, 855-864.
- Lee, C., Martin, R.V., van Donkelaar, A., Lee, H., Dickerson, R.R., Hains, J.C., Krotkov, N., Richter, A., Vinnikov, K., Schwab, J.J., 2011. SO₂ emissions and lifetimes: Estimates from inverse modeling using in situ and global, space-based (SCIAMACHY and OMI) observations. *Journal of Geophysical Research: Atmospheres* 116.
- Lelieveld, J., Crutzen, P.J., Ramanathan, V., Andreae, M.O., Brenninkmeijer, C.A.M., Campos, T., Cass, G.R., Dickerson, R.R., Fischer, H., de Gouw, J.A., Hansel, A., Jefferson, A., Kley, D., de Laat, A.T.J., Lal, S., Lawrence, M.G., Lobert, J.M., Mayol-Bracero, O.L., Mitra, A.P., Novakov, T., Oltmans, S.J., Prather, K.A., Reiner, T., Rodhe, H., Scheeren, H.A., Sikka, D., Williams, J., 2001. The Indian Ocean Experiment: Widespread Air Pollution from South and Southeast Asia. *Science* 291, 1031-1036.
- Mallik, C., Lal, S., Naja, M., Chand, D., Venkataramani, S., Joshi, H., Pant, P., 2013. Enhanced SO₂ concentrations observed over northern India: role of long-range transport. *International Journal of Remote Sensing* 34, 2749-2762.
- Marlier, M.E., DeFries, R.S., Voulgarakis, A., Kinney, P.L., Randerson, J.T., Shindell, D.T., Chen, Y., Faluvegi, G., 2013. El Niño and health risks from landscape fire emissions in southeast Asia. *Nature Climate Change* 3, 131-136.
- Menon, S., Hansen, J., Nazarenko, L., Luo, Y., 2002. Climate effects of black carbon aerosols in China and India. *Science* 297, 2250-2253.
- Mihalopoulos, N., Nguyen, B.C., Boissard, C., Campin, J.M., Putaud, J.P., Belviso, S., Barnes, I., Becker, K.H., 1992. Field study of dimethylsulfide oxidation in the boundary layer: Variations of dimethylsulfide, methanesulfonic acid, sulfur dioxide, non-sea-salt sulfate and aitken nuclei at a coastal site. *Journal of Atmospheric Chemistry* 14, 459-477.

- Millet, D.B., Donahue, N.M., Pandis, S.N., Polidori, A., Stanier, C.O., Turpin, B.J., Goldstein, A.H., 2005. Atmospheric volatile organic compound measurements during the Pittsburgh Air Quality Study: Results, interpretation, and quantification of primary and secondary contributions. *Journal of Geophysical Research: Atmospheres* 110.
- Nair, V.S., Moorthy, K.K., Alappattu, D.P., Kunhikrishnan, P., George, S., Nair, P.R., Babu, S.S., Abish, B., Satheesh, S., Tripathi, S.N., 2007. Wintertime aerosol characteristics over the Indo-Gangetic Plain (IGP): Impacts of local boundary layer processes and long-range transport. *Journal of Geophysical Research: Atmospheres* (1984–2012) 112, doi: 10.1029/2006JD008099.
- Pandis, S.N., Seinfeld, J.H., 2006. *Atmospheric chemistry and physics: From air pollution to climate change*. Wiley.
- Rajput, P., Sarin, M., Sharma, D., Singh, D., 2014a. Characteristics and emission budget of carbonaceous species from post-harvest agricultural-waste burning in source region of the Indo-Gangetic Plain. *Tellus B* 66, doi:10.3402/tellusb.v3466.21026.
- Rajput, P., Sarin, M.M., Sharma, D., Singh, D., 2014b. Organic aerosols and inorganic species from post-harvest agricultural-waste burning emissions over northern India: impact on mass absorption efficiency of elemental carbon. *Environmental Science: Processes & Impacts* 16, 2371-2379.
- Ram, K., Sarin, M.M., 2011. Day–night variability of EC, OC, WSOC and inorganic ions in urban environment of Indo-Gangetic Plain: Implications to secondary aerosol formation. *Atmospheric Environment* 45, 460-468.
- Ramana, M.V., Ramanathan, V., Feng, Y., Yoon, S.C., Kim, S.W., Carmichael, G.R., Schauer, J.J., 2010. Warming influenced by the ratio of black carbon to sulphate and the black-carbon source. *Nature Geosci* 3, 542-545.
- Ramanathan, V., Carmichael, G., 2008. Global and regional climate changes due to black carbon. *Nature Geosci* 1, 221-227.
- Ramanathan, V., Crutzen, P.J., Lelieveld, J., Mitra, A., Althausen, D., Anderson, J., Andreae, M., Cantrell, W., Cass, G., Chung, C., 2001. Indian Ocean Experiment: An integrated analysis of the climate forcing and effects of the great Indo-Asian haze. *Journal of Geophysical Research: Atmospheres* (1984–2012) 106, 28371-28398.
- Rastogi, N., Sarin, M.M., 2006. Chemistry of aerosols over a semi-arid region: Evidence for acid neutralization by mineral dust. *Geophysical Research Letters* 33.
- Rastogi, N., Singh, A., Sarin, M.M., Singh, D., 2015. Temporal variability of primary and secondary aerosols over northern India: Impact of biomass burning emissions. *Atmospheric Environment*.
- Rengarajan, R., Sarin, M.M., Sudheer, A.K., 2007. Carbonaceous and inorganic species in atmospheric aerosols during wintertime over urban and high-altitude sites in North India. *Journal of Geophysical Research: Atmospheres* 112, D21307.
- Saltzman, E., Savoie, D., Prospero, J., Zika, R., 1986. Methanesulfonic acid and non-sea-salt sulfate in Pacific air: Regional and seasonal variations. *Journal of Atmospheric chemistry* 4, 227-240.

- Sarin, M., Kumar, A., Srinivas, B., Sudheer, A., Rastogi, N., 2010. Anthropogenic sulphate aerosols and large Cl-deficit in marine atmospheric boundary layer of tropical Bay of Bengal. *Journal of atmospheric chemistry* 66, 1-10.
- Satheesh, S.K., Moorthy, K.K., Babu, S.S., Vinoj, V., Dutt, C.B.S., 2008. Climate implications of large warming by elevated aerosol over India. *Geophysical Research Letters* 35, n/a-n/a.
- Savoie, D.L., Prospero, J.M., 1989. Comparison of oceanic and continental sources of non-sea-salt sulphate over the Pacific Ocean. *Nature* 339, 685-687.
- Saxena, P., Hildemann, L.M., 1996. Water-soluble organics in atmospheric particles: A critical review of the literature and application of thermodynamics to identify candidate compounds. *Journal of atmospheric chemistry* 24, 57-109.
- Seinfeld, J.H., Carmichael, G.R., Arimoto, R., Conant, W.C., Brechtel, F.J., Bates, T.S., Cahill, T.A., Clarke, A.D., Doherty, S.J., Flatau, P.J., Huebert, B.J., Kim, J., Markowicz, K.M., Quinn, P.K., Russell, L.M., Russell, P.B., Shimizu, A., Shinozuka, Y., Song, C.H., Tang, Y., Uno, I., Vogelmann, A.M., Weber, R.J., Woo, J.-H., Zhang, X.Y., 2004. ACE-ASIA: Regional Climatic and Atmospheric Chemical Effects of Asian Dust and Pollution. *Bulletin of the American Meteorological Society* 85, 367-380.
- Song, J., Zhao, Y., Zhang, Y., Fu, P., Zheng, L., Yuan, Q., Wang, S., Huang, X., Xu, W., Cao, Z., Gromov, S., Lai, S., 2018. Influence of biomass burning on atmospheric aerosols over the western South China Sea: Insights from ions, carbonaceous fractions and stable carbon isotope ratios. *Environmental Pollution* 242, 1800-1809.
- Srivastava, A.K., Ram, K., Pant, P., Hegde, P., Joshi, H., 2012. Black carbon aerosols over Manora Peak in the Indian Himalayan foothills: implications for climate forcing. *Environmental Research Letters* 7, 014002.
- Stein, A., Draxler, R., Rolph, G., Stunder, B., Cohen, M., Ngan, F., 2015. NOAA's HYSPLIT atmospheric transport and dispersion modeling system. *Bulletin of the American Meteorological Society* 96, 2059-2077.
- Sudheer, A.K., Sarin, M.M., 2008. Carbonaceous aerosols in MABL of Bay of Bengal: Influence of continental outflow. *Atmospheric Environment* 42, 4089-4100.
- Sullivan, A.P., Weber, R.J., 2006. Chemical characterization of the ambient organic aerosol soluble in water: 1. Isolation of hydrophobic and hydrophilic fractions with a XAD-8 resin. *Journal of Geophysical Research: Atmospheres* 111.
- Thamban, N.M., Tripathi, S.N., Moosakutty, S.P., Kuntamukkala, P., Kanawade, V.P., 2017. Internally mixed black carbon in the Indo-Gangetic Plain and its effect on absorption enhancement. *Atmospheric Research* 197, 211-223.
- Turpin, B.J., Lim, H.-J., 2001. Species contributions to PM_{2.5} mass concentrations: Revisiting common assumptions for estimating organic mass. *Aerosol Science & Technology* 35, 602-610.
- Venkataraman, C., Habib, G., Eiguren-Fernandez, A., Miguel, A., Friedlander, S., 2005. Residential biofuels in South Asia: carbonaceous aerosol emissions and climate impacts. *Science* 307, 1454-1456.

Wang, Y., Zhuang, G., Zhang, X., Huang, K., Xu, C., Tang, A., Chen, J., An, Z., 2006. The ion chemistry, seasonal cycle, and sources of PM_{2.5} and TSP aerosol in Shanghai. *Atmospheric Environment* 40, 2935-2952.

Wu, C., Yu, J.Z., 2016. Determination of primary combustion source organic carbon-to-elemental carbon (OC/EC) ratio using ambient OC and EC measurements: secondary OC-EC correlation minimization method. *Atmos. Chem. Phys.* 16, 5453-5465.

Xiang, P., Zhou, X., Duan, J., Tan, J., He, K., Yuan, C., Ma, Y., Zhang, Y., 2017. Chemical characteristics of water-soluble organic compounds (WSOC) in PM_{2.5} in Beijing, China: 2011–2012. *Atmospheric Research* 183, 104-112.

Xiao, H.-Y., Liu, C.-Q., 2004. Chemical characteristics of water-soluble components in TSP over Guiyang, SW China, 2003. *Atmospheric Environment* 38, 6297-6306.

Yao, X., Chan, C.K., Fang, M., Cadle, S., Chan, T., Mulawa, P., He, K., Ye, B., 2002. The water-soluble ionic composition of PM_{2.5} in Shanghai and Beijing, China. *Atmospheric Environment* 36, 4223-4234.

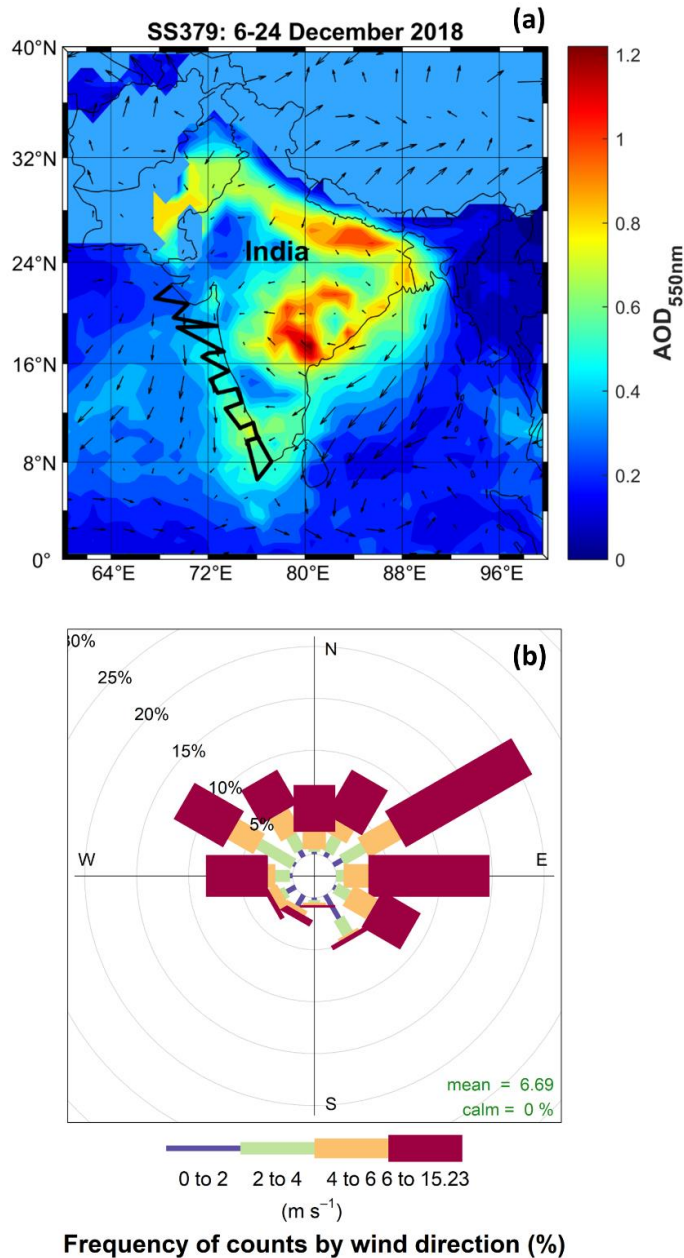
Youn, J.-S., Wang, Z., Wonaschütz, A., Arellano, A., Betterton, E.A., Sorooshian, A., 2013. Evidence of aqueous secondary organic aerosol formation from biogenic emissions in the North American Sonoran Desert. *Geophysical Research Letters* 40, 3468-3472.

Zhang, G.S., Zhang, J., Liu, S.M., 2007. Chemical composition of atmospheric wet depositions from the Yellow Sea and East China Sea. *Atmospheric Research* 85, 84-97.

Zhang, H.-H., Yang, G.-P., Liu, C.-Y., Su, L.-P., 2013. Chemical Characteristics of Aerosol Composition over the Yellow Sea and the East China Sea in Autumn*. *Journal of the Atmospheric Sciences* 70, 1784-1794.

Zhang, Q., Sarkar, S., Wang, X., Zhang, J., Mao, J., Yang, L., Shi, Y., Jia, S., 2019. Evaluation of factors influencing secondary organic carbon (SOC) estimation by CO and EC tracer methods. *Science of The Total Environment* 686, 915-930.

Figure 1. (a) Cruise track in the Arabian Sea during SS379 cruise (6-24 December 2018) along with a background of MODIS satellite-based aerosol optical depth (AOD) values at 550 nm and surface winds at 10 m height from NOAA meteorological datasets, (b) typical wind rose showing the wind direction and speed obtained from the AWS data during the cruise period



[§]Equivalent mass ratio; [§]#SO₄²⁻ concentration excludes contribution from biogenic DMS and seasalt.

Table 1. Statistical summary of the chemical composition of TSP collected over the Arabian Sea during SS379 cruise (6-26 December 2018).

Species/Components	Concentrations ($\mu\text{g m}^{-3}$)
	Min-Max (Av \pm Sd)
Na ⁺	1.2-4.7(2.8 \pm 1.1)
NH ₄ ⁺	0.3-5.8 (2.0 \pm 1.5)
K ⁺	0.4-1.5(0.7 \pm 0.3)
Ca ²⁺	0.1-3.6 (1.1 \pm 0.9)
Mg ²⁺	0.1-0.7(0.4 \pm 0.2)
MSA	0.02-0.12 (0.05 \pm 0.03)
Cl ⁻	0.5-4.0 (2.0 \pm 1.0)
NO ₃ ⁻	0.8-3.8(2.0 \pm 0.8)
SO ₄ ²⁻	3.0-16.4(9.4 \pm 3.9)
nss-SO ₄ ²⁻	2.5-15.8 (8.7 \pm 3.9)
anthropogenic-SO ₄ ²⁻	2.2-15 (8.0 \pm 3.9)
nss-K ⁺	0.3 - 1.5 (0.6 \pm 0.3)
nss-Ca ²⁺	0.05-3.4 (1.0 \pm 0.9)
OC	3.0 - 15.7 (6.7 \pm 3.3)
EC	0.5 - 2.4 (1.4 \pm 0.5)
WSOC	1.5-7.8 (3.7 \pm 1.5)
OC/EC	2.5-10.5 (4.9 \pm 1.8)
WSOC/OC	0.30-0.74 (0.59 \pm 0.12)
WIOC/EC	0.65-7.38 (2.16 \pm 1.51)
[§] NH ₄ ⁺ /SO ₄ ²⁻	0.18-1.01 (0.55 \pm 0.25)
[#] NO ₃ ⁻ /SO ₄ ²⁻	0.09-0.65 (0.31 \pm 0.19)
nss-K ⁺ /EC	0.14-1.18 (0.45 \pm 0.26)
nss-K ⁺ /OC	0.03-0.29(0.10 \pm 0.07)
nss-SO ₄ ²⁻ /EC	2.5-12.6(6.8 \pm 3.0)
nss-SO ₄ ²⁻ /nss-Ca ²⁺	2-199(31 \pm 52)
nss-K ⁺ /nss-Ca ²⁺	0.13-9.3(1.7 \pm 2.6)

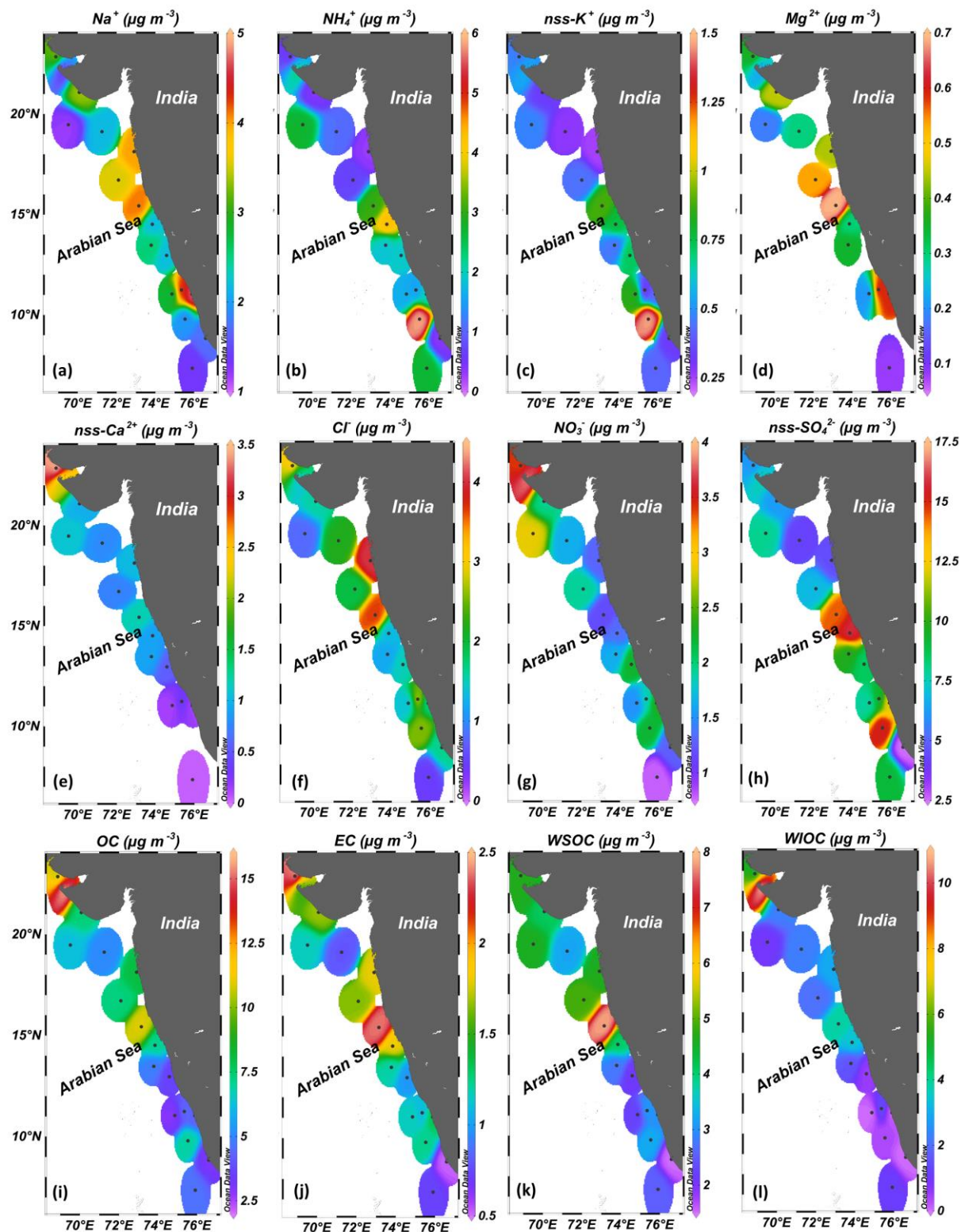


Figure 2. Spatial variability of mass concentrations of (a-h) water-soluble inorganic ions, (i) organic carbon: OC, (j) elemental carbon: EC, (k) water-soluble organic carbon: WSOC (l) water-insoluble organic carbon: WIOC in TSP collected during SS379 cruise in the Arabian Sea.

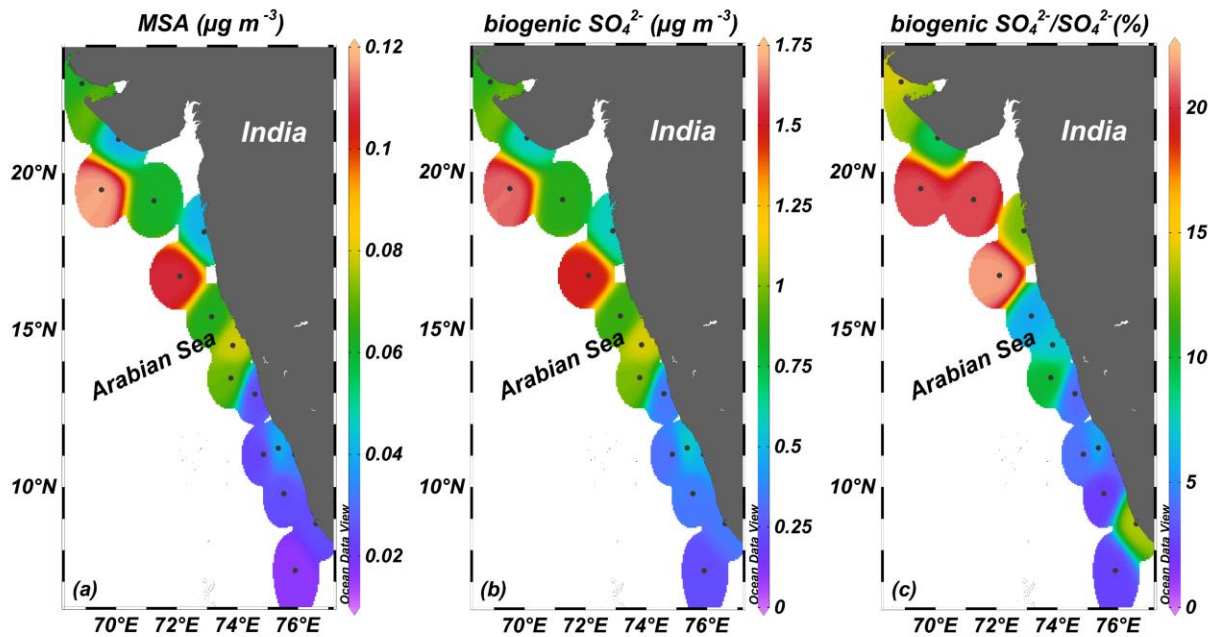


Figure 3. Latitudinal variability of atmospheric concentrations of (a) methanesulfonic acid (MSA), (b) biogenic SO_4^{2-} , and (c) the ratio of biogenic SO_4^{2-} to non-sea-salt SO_4^{2-} in TSP collected over the Arabian Sea during SS379 cruise (6 – 26 December 2018).

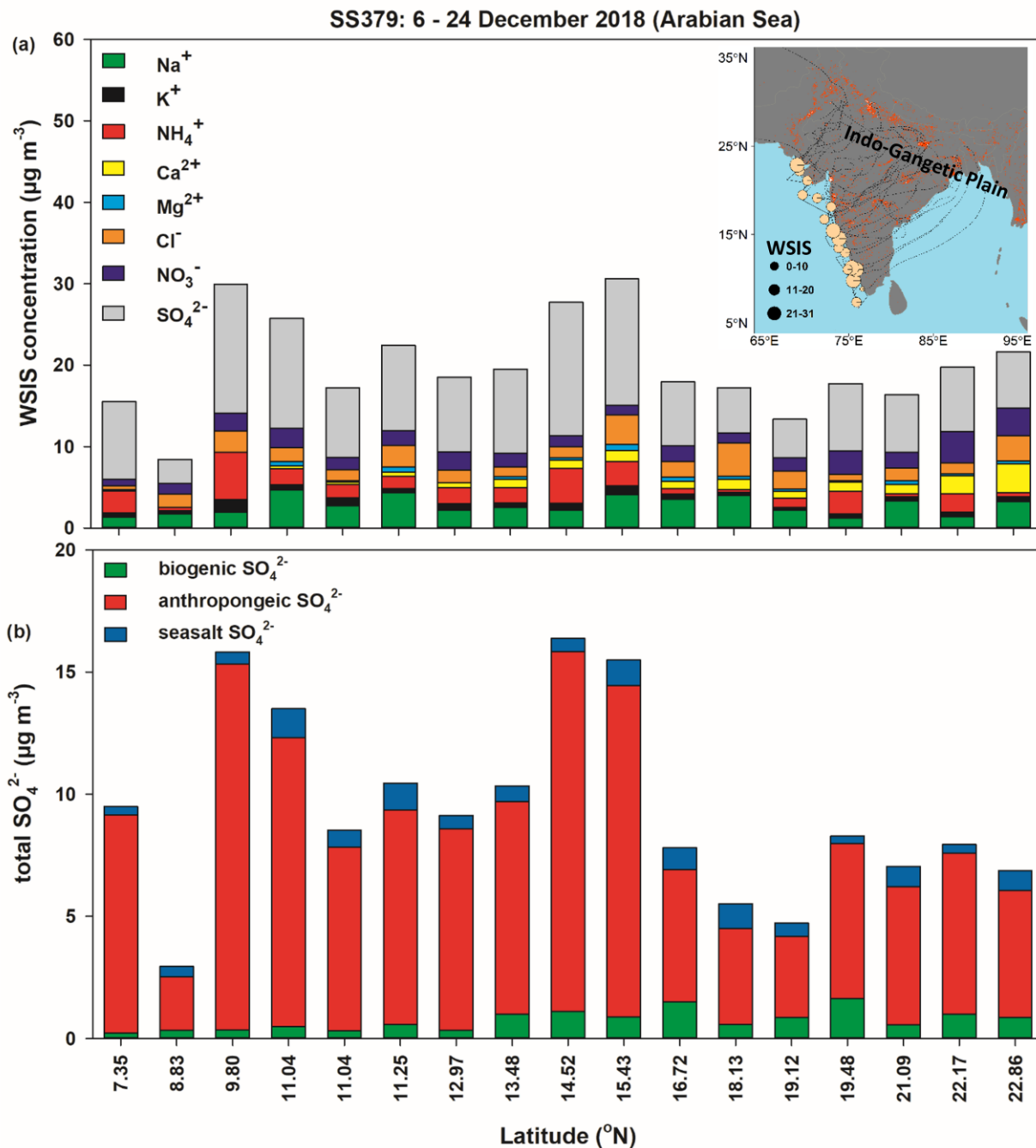


Figure 4. Latitudinal variability of relative abundances of water-soluble inorganic species in their total mass concentration in TSP samples collected over the Arabian Sea during SS379 cruise (6-24 December 2018). The inset shows the spatial variability of TSP concentrations over the Arabian Sea along with MODIS fire counts (red dots) and 7-day HYSPLIT backward air mass trajectories (dashed lines) during the SS379 cruise. In the inset of panel (a), WSIS is expressed in $\mu\text{g m}^{-3}$.

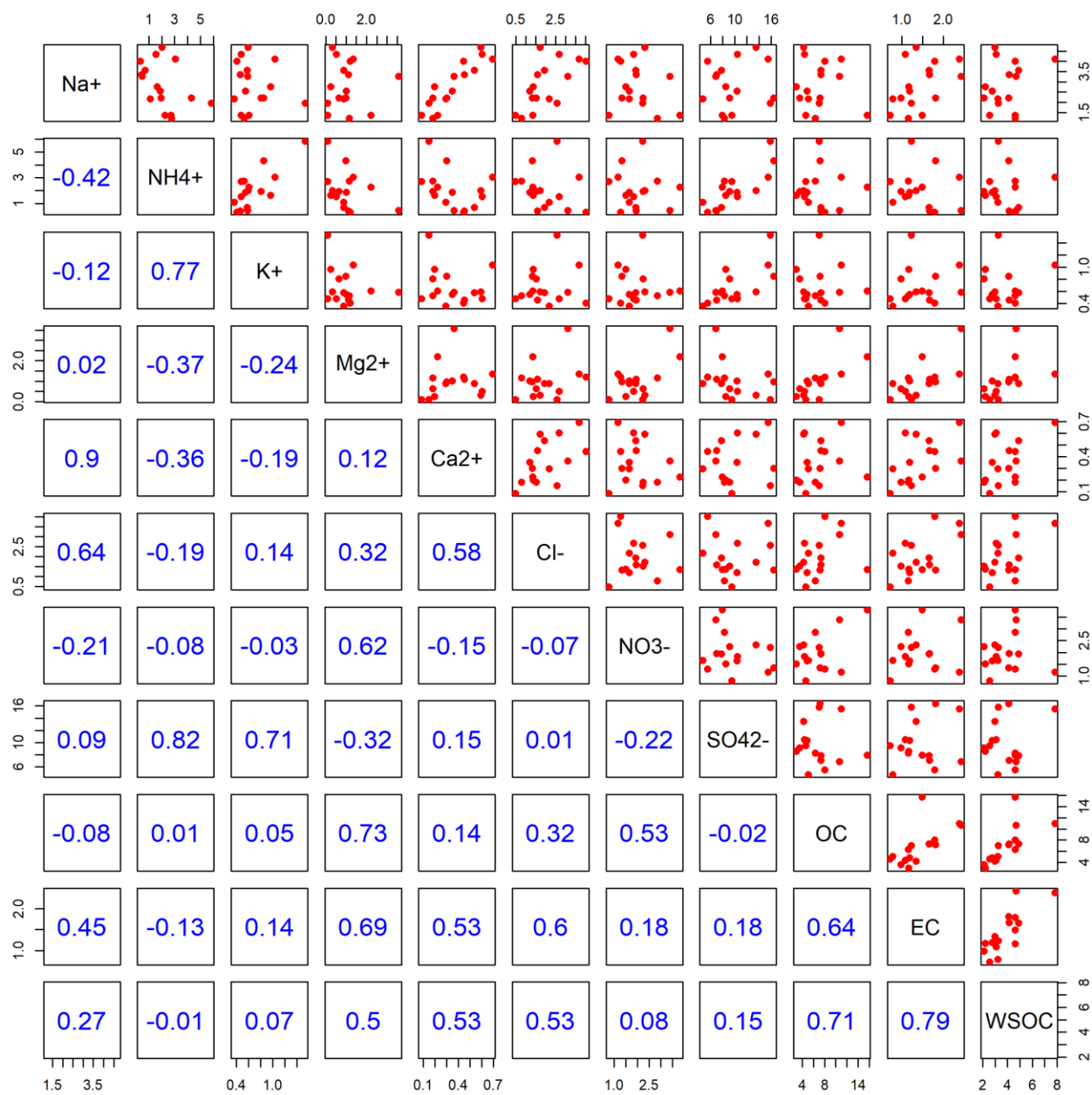


Figure 5. Pearson's correlation matrix of water-soluble inorganic species and carbonaceous components in TSP samples collected over the Arabian Sea during the SS379 cruise (6-24 December 2018). Here, the bottom diagonal triangle values provided below the chemical species are the correlation coefficient (r). Also, Pearson's critical- r value for the sample size of SS379 cruise is 0.48 (i.e., ' r ' \geq 0.49 are significant).

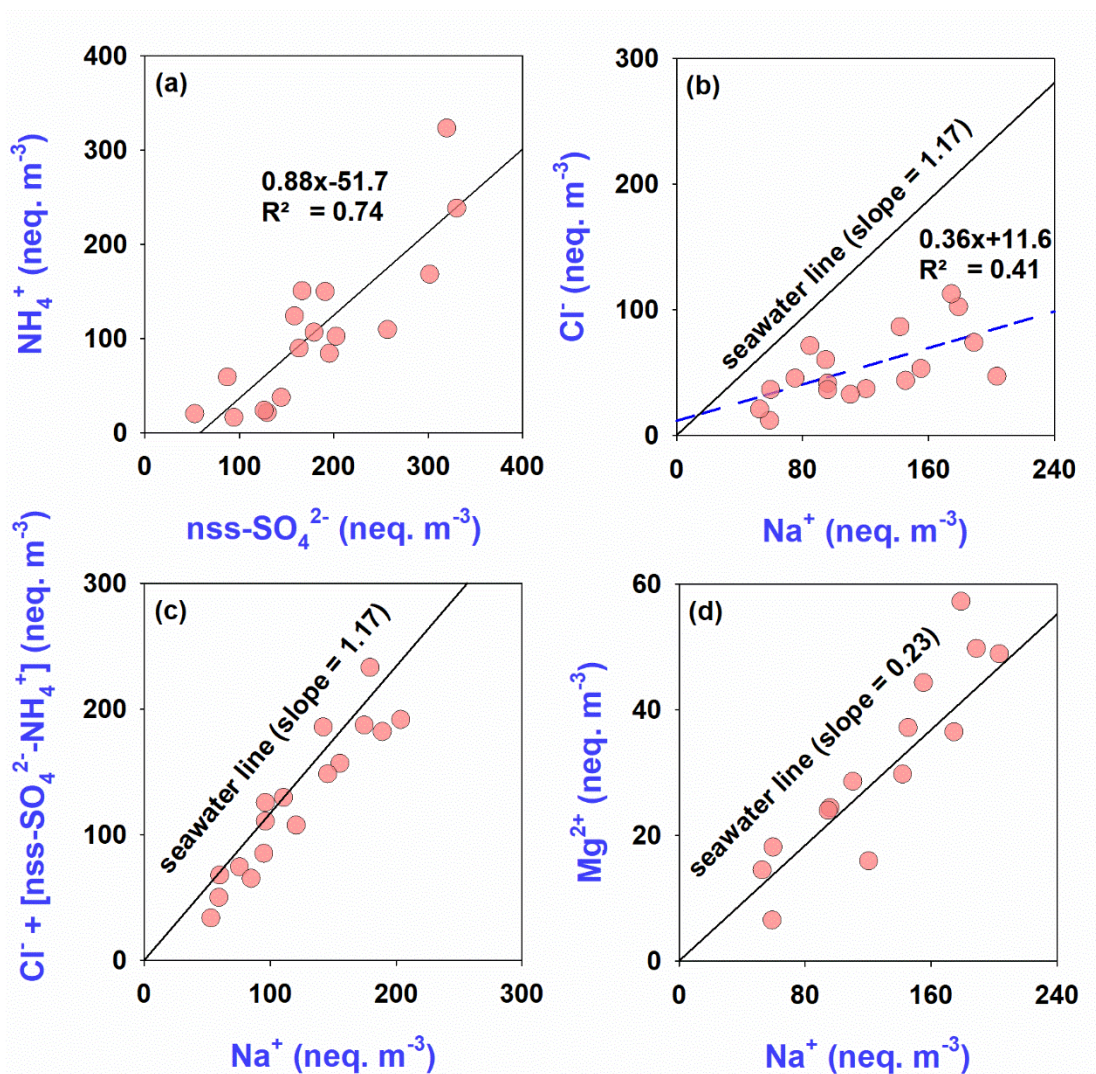


Figure 6. Linear regression analysis between equivalent mass concentrations of (a) non-sea-salt or nss-SO_4^{2-} and NH_4^+ , (b) Na^+ and Cl^- , (c) Na^+ and Cl^- plus excess SO_4^{2-} , and (d) Na^+ and Mg^{2+} in TSP samples collected over Arabian Sea during SS379 cruise (6-24 December 2018).

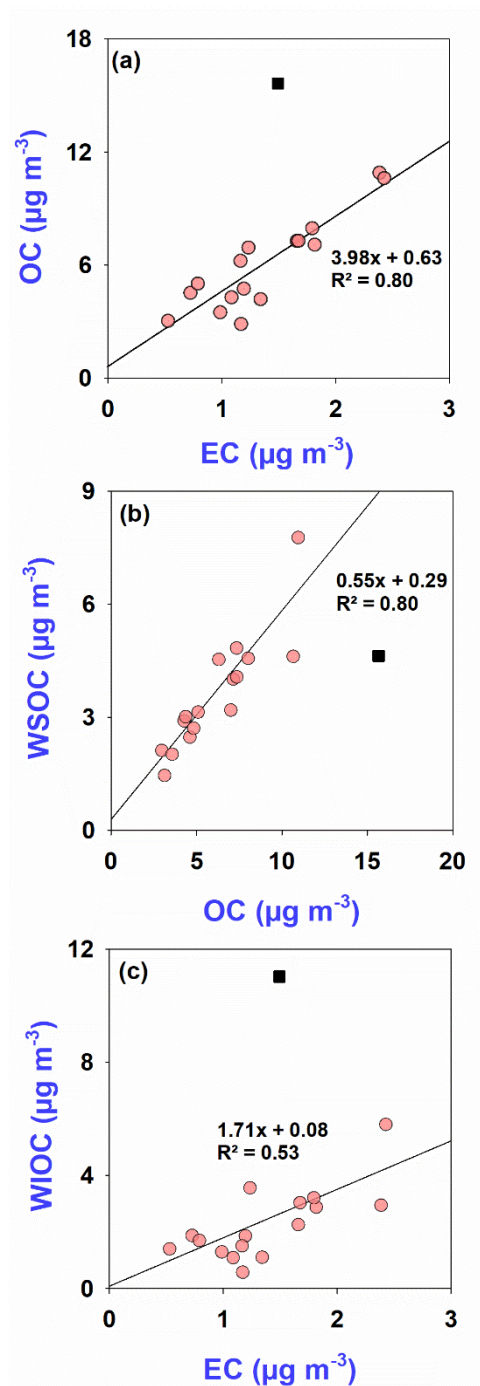


Figure 7. Linear regression analysis between mass concentrations of (a) OC and EC, (b) OC and WSOC, (c) Na^+ and Cl^- plus excess SO_4^{2-} , and (d) Na^+ and Mg^{2+} in TSP samples collected over the Arabian Sea during SS379 cruise (6-24 December 2018).

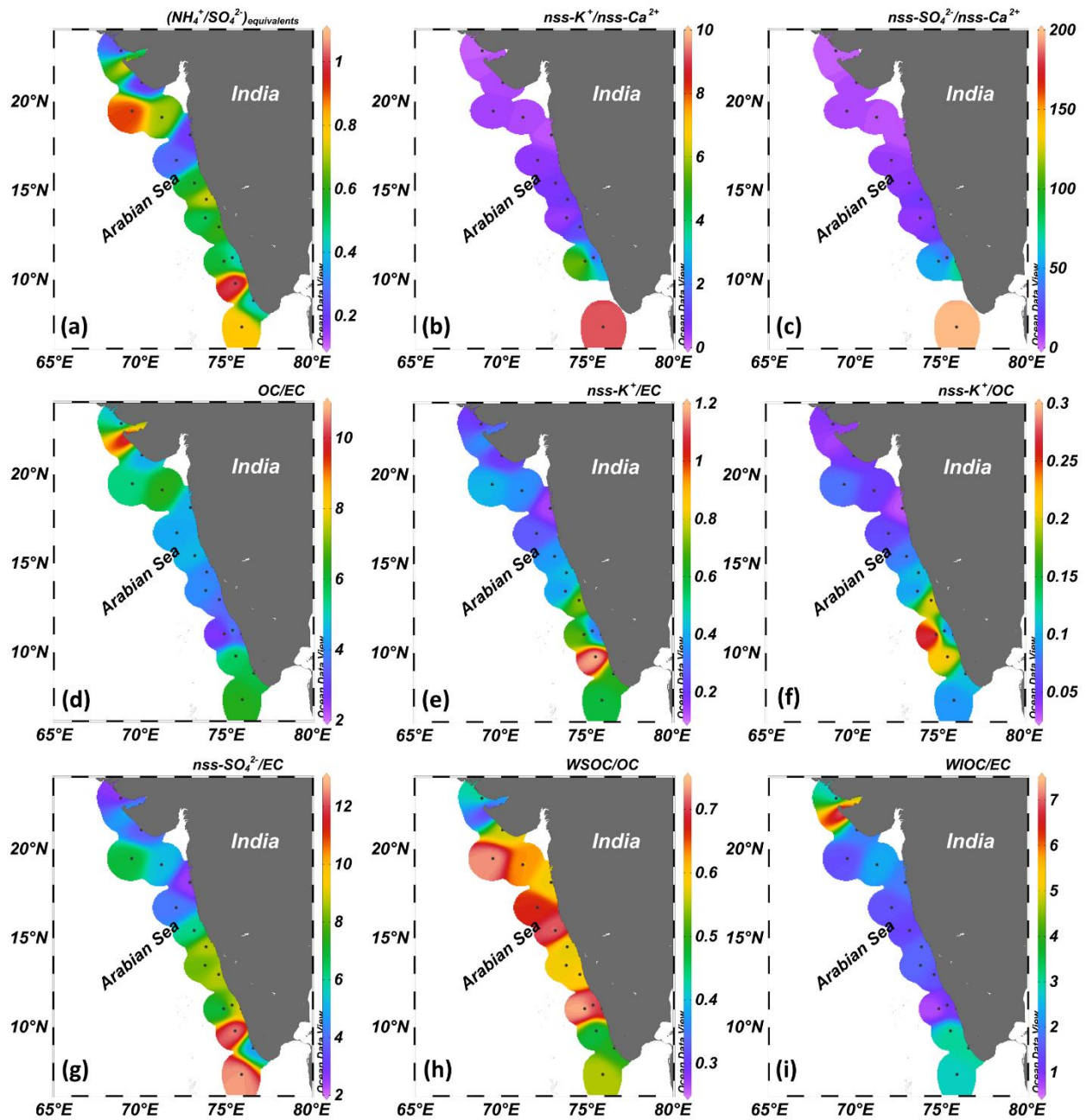


Figure 8. Diagnostic mass ratios of chemical constituents measured in TSP samples collected over the Arabian Sea during SS379 cruise (6-24 December 2018).

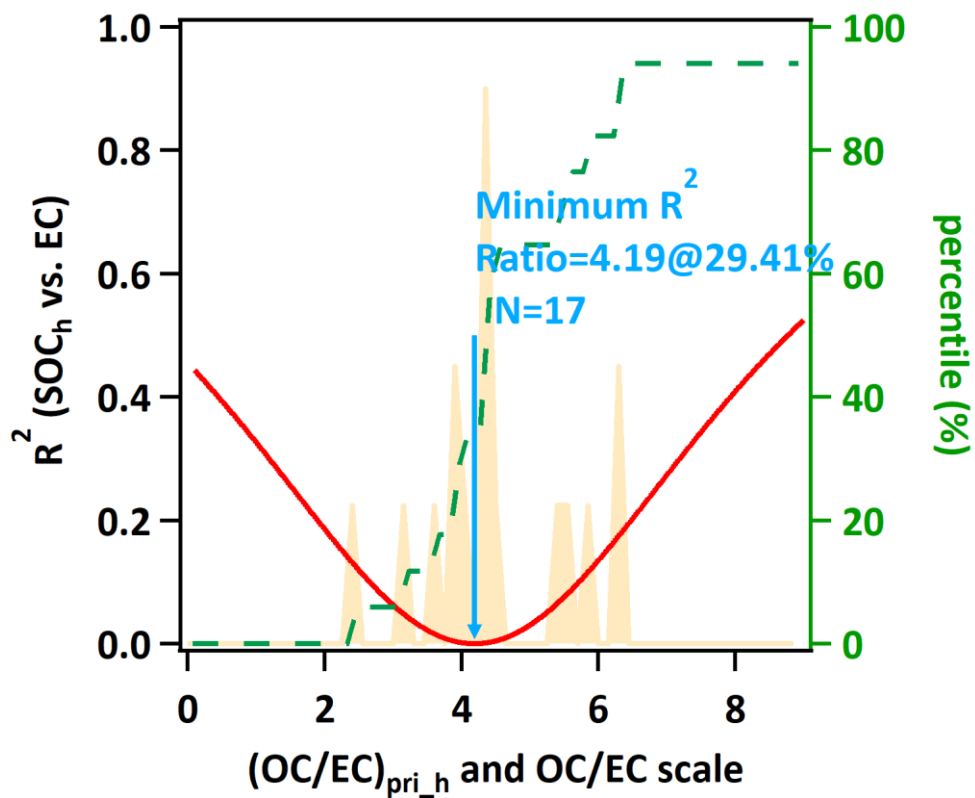


Figure 9. Estimate of primary OC/EC ratio from the emissions by the minimum R^2 method (MRS) for the TSP collected over the Arabian Sea during SS379 cruise (6-24 December 2018).

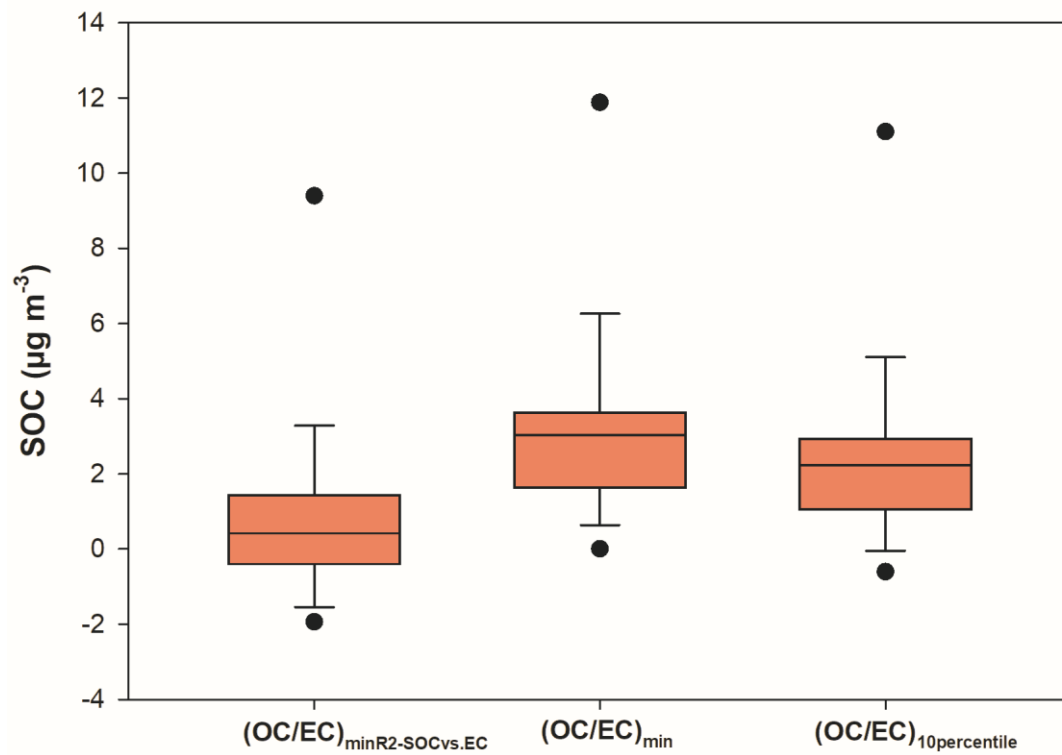


Figure 10. Estimate of primary OC/EC ratio from the emissions by the minimum R^2 method (MRS) for the TSP collected over the Arabian Sea during SS379 cruise.

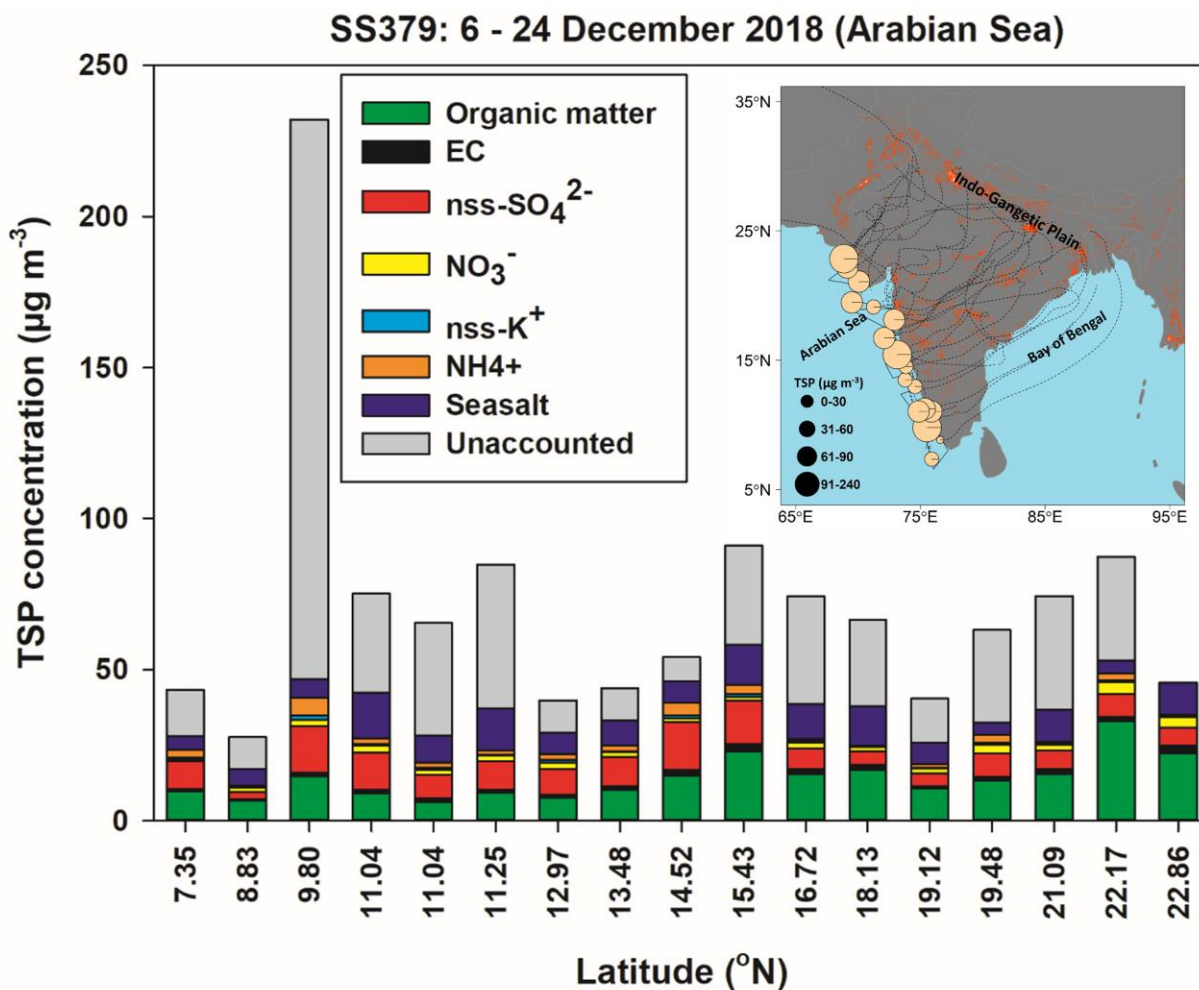


Figure 11. Latitudinal variability of relative abundances of water-soluble inorganic species (WSIS), organic matter (OC \times 2.0), elemental carbon (EC), sea salt ($\text{Na}^+ \times 3.2$), and the unaccounted mass loading of TSP concentrations obtained over the Arabian Sea during SS379 cruise. Here, the factor 2.0 accounts for the oxidation of organic matter during long-range transport from the IGP and 3.2 is the weight ratio of salinity to sodium in seawater (Bikkina et al., 2014). The inset shows the spatial variability of TSP concentrations over the Arabian Sea along with MODIS fire counts (red dots) and 7-day HYSPLIT backward air mass trajectories (dashed lines) during the SS379 cruise.

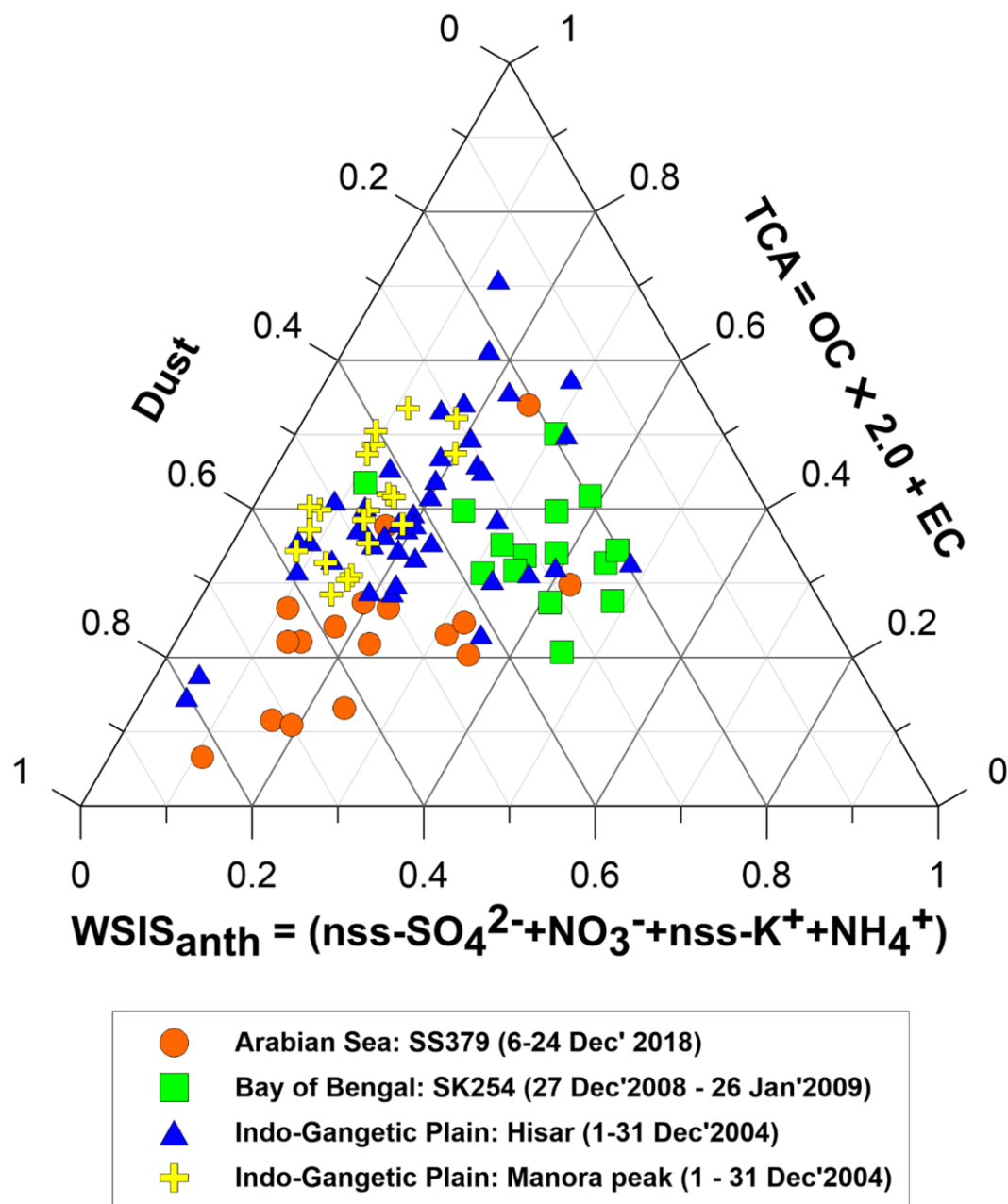


Figure 12. Ternary plot for comparison of relative abundances of anthropogenic water-soluble inorganic species ($WSIS_{anth}$), total carbonaceous aerosol mass loading (TCA), and the estimated dust concentrations (*i.e.*, $TSP - TCA - WSIS_{anth}$) over the Arabian Sea with those reported over the Bay of Bengal (Bikkina and Sarin, 2012) and the urban (Hisar, Haryana; 219 m asl; (Rengarajan et al., 2007) and remote high altitude receptor sites (Manora peak, Uttarakhand; 1950 m asl; (Rengarajan et al., 2007)) in the IGP.

Supporting information for

Chemical characterization of wintertime marine aerosols over the Arabian Sea: impact of marine sources and long-range transport

Coauthored by

Poonam Bikkina^{1,*}, V.V.S.S. Sarma¹, Kimitaka Kawamura², Srinivas Bikkina², Bhagawati Kunwar², Sherin C.K.³

¹CSIR-National Institute of Oceanography, Regional Centre, Visakhapatnam 530017, Andhra Pradesh, India

²Chubu University, Kasugai-shi, Aichi, 487-8501, Japan

³Center for Marine Living Resources and Ecology, Kochi 682508, Kerala, India

Contents of the file:

Figure S1-Figure S2

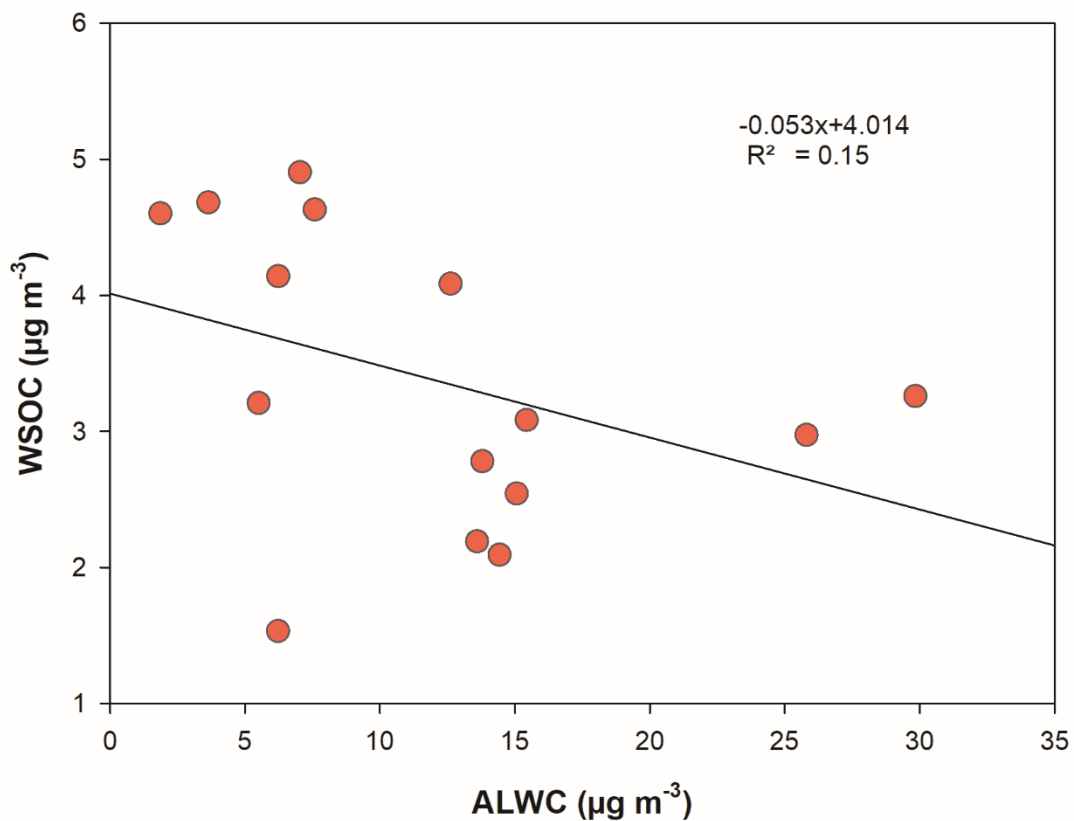


Figure S1: Relationship between aerosol liquid water content (ALWC), estimated from the thermodynamic equilibrium partition model (ISORROPIA-II), and WSOC in TSP collected over the Arabian Sea during SS379 cruise.

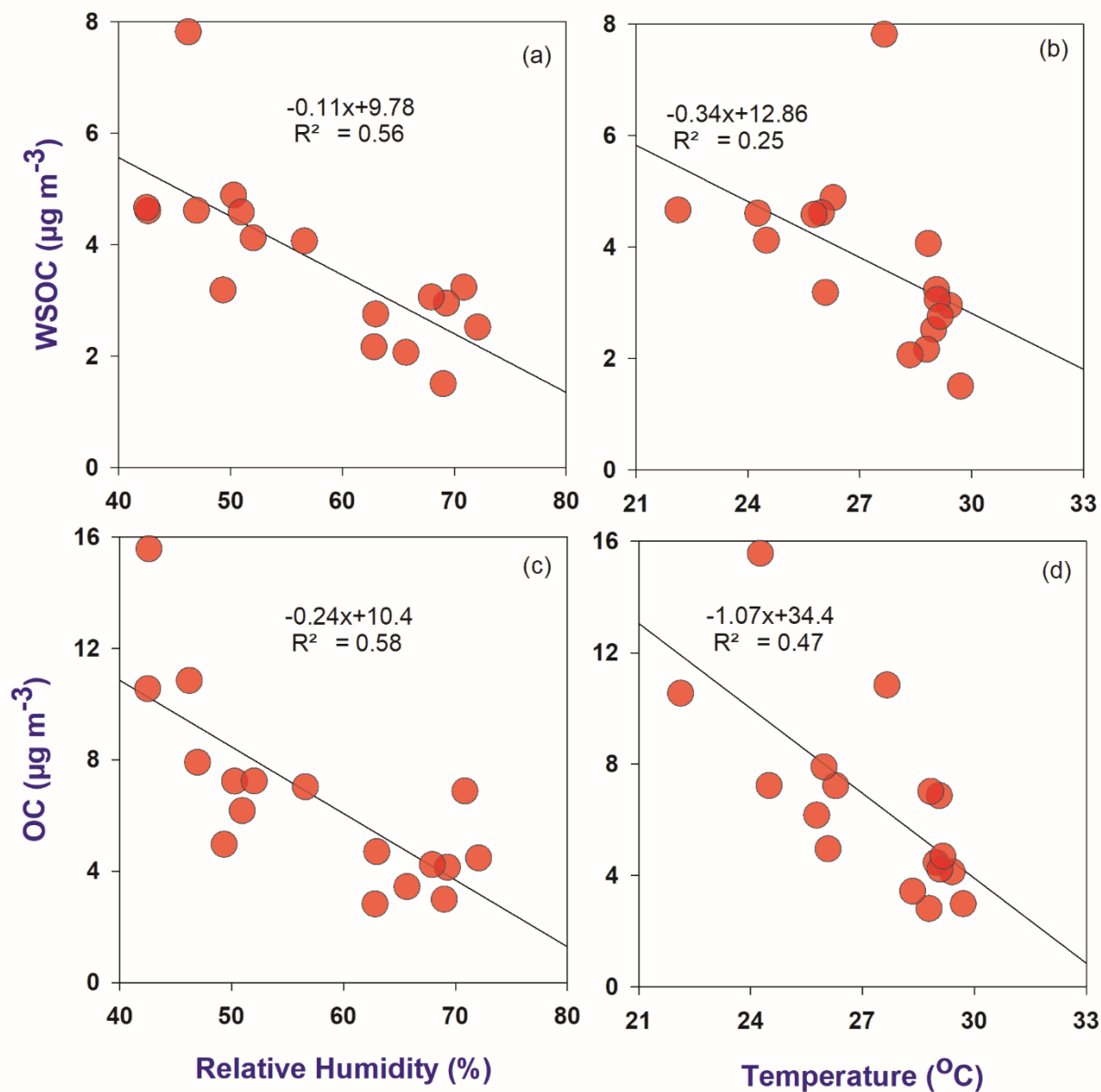


Figure S2: Scatterplot of relative humidity and temperature with WSOC (a-b), and OC (c-d) in TSP samples collected over the Arabian Sea during SS379 cruise.